Scattering Properties of Aerosols in Clean Marine and Polluted Air

A Thesis Presented to
The National University of Ireland, Galway
For the Degree of Doctor of Philosophy

By

Aditya Vaishya

Supervisor: **Professor Colin O'Dowd**

School of Physics,
National University of Ireland Galway,
Galway, Ireland.

June, 2012

Table of Contents

Abstract

The light scattering properties of aerosols are affected by their chemical composition, size distribution and ambient relative humidity (*RH*) thus making them highly variable in both the spatial and temporal domains, which induces large uncertainty in their radiative effects on climate. Long-term aerosol measurements are key for developing a better understanding of their radiative properties. In the pristine marine environment, sea-spray aerosols are the precursors for cloud formation, which then act as a reflecting layer for incoming solar radiation. This increases the overall albedo of the marine environment, thus inducing a cooling effect on the climate which otherwise is towards warming because of the darker ocean surface. The main factors which influence the production mechanisms and radiative properties of sea-spray aerosols are wind-speed, relative humidity and ocean near-surface layer chemical composition which in turn show seasonal behaviour. Hence it is vital to study the radiative properties of sea-spray aerosols with reference to these influencing parameters in order to reduce uncertainties in the estimation of the Earth's radiation budget and to obtain more reliable climate predictions.

In the present work, the scattering properties of sea-spray aerosols with reference to above mentioned variables were investigated for clean marine air masses arriving at the Mace Head Atmospheric Research Station on the western periphery of Europe. Ten years (2001-2010) of aerosol light scattering data showed a clear seasonal trend in the aerosol light scattering coefficient (σ_{scat}) and the Ångström exponent ($\mathring{A}$). σ_{scat} values were maximum (35.3 Mm^{-1}) in the month of January and minimum (13.7 Mm^{-1}) in the month of July. A high positive correlation coefficient of 0.82 was also found for the summer season between percentage occurrence of lower σ_{scat} values (5-15 Mm^{-1}) and the percentage occurrence of relatively large $\mathring{A}$ values (>1.2). A high positive correlation coefficient of 0.88 was found between wind-speed and σ_{scat}. These

findings clearly indicate that high σ_{scat} values in the winter season are due to the contribution of wind driven sea-spray aerosols in the marine boundary layer. Subsequent studies found that σ_{scat} and the aerosol light backscattering coefficient (σ_{bscat}) are dependent on the square of wind-speed ~ U^2. It was also found that σ_{scat} for the low biological activity (LBA) period was approximately twice that found for the high biological activity (HBA) period. This difference was attributed to the combined effect of size distribution and refractive index whereas refractive index on its own accounted for 70% of the observed differences.

A relative humidity (*RH*) scanning Nephelometer (Humidograph) instrument was built to study the effect of *RH* on aerosol light scattering properties. It was found that the aerosol light scattering enhancement (*f(RH)*) values for the clean marine air masses was 2.22 at 85% *RH* which is higher than the *f(RH)* value 1.77 for polluted air masses. Also, the effect of *RH* on backscatter fraction and single scattering albedo was to reduce the former by 20% and to increase the latter by 1-5% at 85% *RH* as compared to dry conditions. By combining the information about aerosol chemical composition and hygroscopic growth factor (*HGF*), a new *HGF* parameterization for sea-spray aerosols was established. Using the *HGF* parameterization along with aerosol density and refractive index as inputs to a Mie radiative code, a dual hygroscopicity state, flipping from high-hygroscopicity and high *f(RH)* to low-hygroscopicity and low *f(RH)*, of aerosol was found as the organic matter mixing volume percentage exceeded ~ 50%. The effect of organic enrichment on the top of atmosphere (*TOA*) direct radiative forcing (ΔF) was to reduce the cooling contribution of sea-spray aerosol by ~4.5 times as compared to pure sea-salt spray.

The work presented in this thesis has quantified the effects of relative humidity, wind-speed, and aerosol chemical composition on its radiative properties, thus helping to address some key questions pertaining to marine aerosols.

Acknowledgements

First and foremost, I gratefully acknowledge the guidance and support of Prof. Colin O'Dowd. His sound advice, analytical and scientific approach has been of great help to me throughout my PhD.

The good advice and support of my co-supervisor, Prof. (Emeritus) S. G. Jennings, has been invaluable on both an academic and a personal level, for which I am extremely grateful.

It was a great pleasure to be in the C-CAPS group. I would like to thank my colleagues and friends in the group for all those wonderful (scientific) discussions, and lunch and coffee breaks. Brendan Kelly deserves special thanks for his technical support in the development of the Wet-Neph instrument. Thanks to the technical staff at the School of Physics workshop for their help in giving a shape to the instrument.

I thank my housemate-friends who provided such a lovely and homely atmosphere and my friends in Ireland, for their wonderful company throughout my PhD.

Finally, I would like to thank my family and friends in India for their love and support. Papa and Amma without your love and blessings I would not have accomplished this. My Alfa-5 brothers for their love and encouragement. My Mother-in law and my extended family for being supportive and understanding. My lovely, caring, and patient wife, Megha, without whom I would not have started this PhD.

List of Research Papers

This thesis consists of an introduction of the subject, overview of peer-reviewed published research articles followed by full research articles and conclusions drawn from the present work.

1. **Vaishya A.**, S.G. Jennings, C. O'Dowd (2011), Seasonal variation of the aerosol light scattering coefficient in marine air of the Northeast Atlantic, *Adv. Meteorol.*, *vol. 2011*, Article ID 170490, doi:10.1155/2011/170490.

2. **Vaishya A.**, S.G. Jennings, C. O'Dowd (2012), Wind-driven influences on aerosol light scattering in North-East Atlantic air, *Geophy. Res. Lett.*, 39, L05805, doi:10.1029/2011GL050556.

3. Fierz-Schmidhauser R., P. Zieger, **A. Vaishya**, C. Monahan, J. Bialek, C.D. O'Dowd, S.G. Jennings, U. Baltensperger, E. Weingartner (2010), Light scattering enhancement factors in the marine boundary layer (Mace Head, Ireland), *J. Geophys. Res.*, 115 (20), D20204, doi:10.1029/2009JD013755.

4. **Vaishya A.**, J. Ovadnevaite, J. Bialek, S.G. Jennings, D. Ceburnis, C. O'Dowd, Warming or cooling? The flippant effect of organics on sea-spray light-scattering, Submitted to *Nature Geoscience*.

5. O'Dowd C.D., D. Ceburnis, J. Ovadnevaite, G. Martucci, J. Bialek, C. Monahan, H. Berresheim, **A. Vaishya**, T. Grigas, S.G. Jennings, P. McVeigh , S. Varghese, R. Flanagan, D. Martin, E. Moran, K. Lambkin, T. Semmler, C. Perrino, R. McGrath (2011), The Eyjafjallajökull ash plume Part I: Physical, chemical and optical characteristics, *Atmos. Environ.,* 48, 129 – 142, doi:10.1016/j.atmosenv.2011.07.004.

6. O'Dowd C.D., S. Varghese, D. Martin, R. Flanagan, D. Ceburnis, J. Ovadnevaite, G. Martucci, J. Bialek, C. Monahan, H. Berresheim, **A. Vaishya**, T. Grigas, Z. McGraw, S.G. Jennings, B. Langmann, T. Semmler, R. McGrath (2011), The Eyjafjallajökull ash plume Part 2: Simulating ash cloud dispersion with REMOTE, *Atmos. Environ.,* 48, 143 – 151, doi:10.1016/j.atmosenv.2011.10.037.

1. Introduction

The term aerosol refers to a dispersion of solid and/or liquid particles suspended in air. This definition applies generally to include haze, smog, fog, smoke, and dust. Smoke, smog and dust consists of particulate matter, haze and fog consists of solid material in solution or suspension in water droplets. Atmospheric aerosols have diverse natural and anthropogenic origins and their production mechanisms involve a vast array of physical and chemical processes [*Prospero*, 1983]. Examples of natural origin aerosols are: mineral dust aerosol that is emitted by the effects of wind erosion on arid land [*Dentener et al.*, 2006], sea-spray particles produced via bubble bursting processes [*Blanchard and Woodcock*, 1957], and ash particles ejected during volcanic eruptions [*Robock*, 2000]. Examples of anthropogenic aerosols are black carbon and sulphate from industrial sources and combustion of fossil fuels [*Penner et al.*, 1998], and aerosols from biomass burning [*Andreae and Merlet*, 2001]. Based on their production mechanism, aerosols are classified as primary in origin (emitted directly at source) or secondary in origin (formed from gaseous precursors by various gas and aqueous phase oxidation processes). Examples of primary aerosols include: sea-salt particles emitted at the ocean surface, mineral dust aerosol emitted by the effects of wind erosion on arid land, and ash particles from industrial activities. Examples of secondary aerosols are sulphate aerosol that is formed from sulphur emissions from fossil fuel burning and aerosol formation from dimethyl sulphide (DMS) emissions by marine phytoplankton.

Quantification of global emissions of natural and anthropogenic aerosols is obtained using general circulation climate models (GCM) in conjunction with emissions inventories. Natural aerosols are by far the largest in terms of global emission with emissions of the order of few thousands of Teragram (Tg) per year as compared to anthropogenic aerosols with emission estimates of a few hundred Tg y^{-1}. Two predominant natural sources of aerosols in terms of global emission

estimates are sea-spray, with global emission estimates of 6297 Tg y^{-1} [*Vignati et al.*, 2010], and dust aerosols, with global emission estimates of 1776 Tg y^{-1} [*Dentener et al.*, 2006]. This is followed by secondary organic aerosols (~ 19 Tg y^{-1} [*Dentener et al.*, 2006]), volcanic aerosols (12 Tg y^{-1} [*Dentener et al.*, 2006]), and DMS (18.46 Tg y^{-1} [*Kettle et al.*, 1999]). Dominant anthropogenic aerosols are sulphate from industry (~ 69 Tg y^{-1} [*Cofala et al.*, 2007]) and black carbon from fossil fuel burning (4.5 Tg C y^{-1} [*Andreae and Rosenfeld*, 2008]).

Aerosol size ranges from a few nanometres to hundreds of micrometers (μm). The size distribution is thus classified in different size modes, which are based on their formation, transformation and removal processes. Two main categories are: coarse mode (particle diameter D >2.5 μm) and fine mode (D < 2.5 μm) [*Whitby*, 1978], which are classified based on their production and removal mechanisms. Fine mode is further classified into nucleation mode (D < 10 nm), Aitken mode (10 nm < D < 100 nm) and accumulation mode (0.1 μm < D < 2.5 μm). Nucleation and Aitken mode particles are formed by condensation of gases or are directly emitted at source. Accumulation mode particles are formed by coagulation and condensational growth of smaller particles. Coarse mode particles are formed by mechanical processes and are primary in origin as opposed to fine mode particles which in general are secondary in origin.

In the subsequent sections, climatic effects of aerosols are discussed followed by the importance of natural aerosols and specifically marine aerosols. Further to this, factors influencing the optical properties of atmospheric aerosols are elaborated upon. This is followed by a set of questions pertaining to marine aerosols. Addressing these questions forms the main basis of the thesis.

1.1. Climatic effects of aerosols

Aerosols play an important role in the dynamic atmospheric system. Anthropogenic aerosols influence visibility by forming haze layers. Figure 1.1a shows the famous Petronas Towers (the tallest twin buildings ever built), in Kuala Lumpur, Malaysia. The valley and the mountains in the background are sharp and clearly visible in contrast to Figure 1.1b where visibility is reduced due to haze layers.

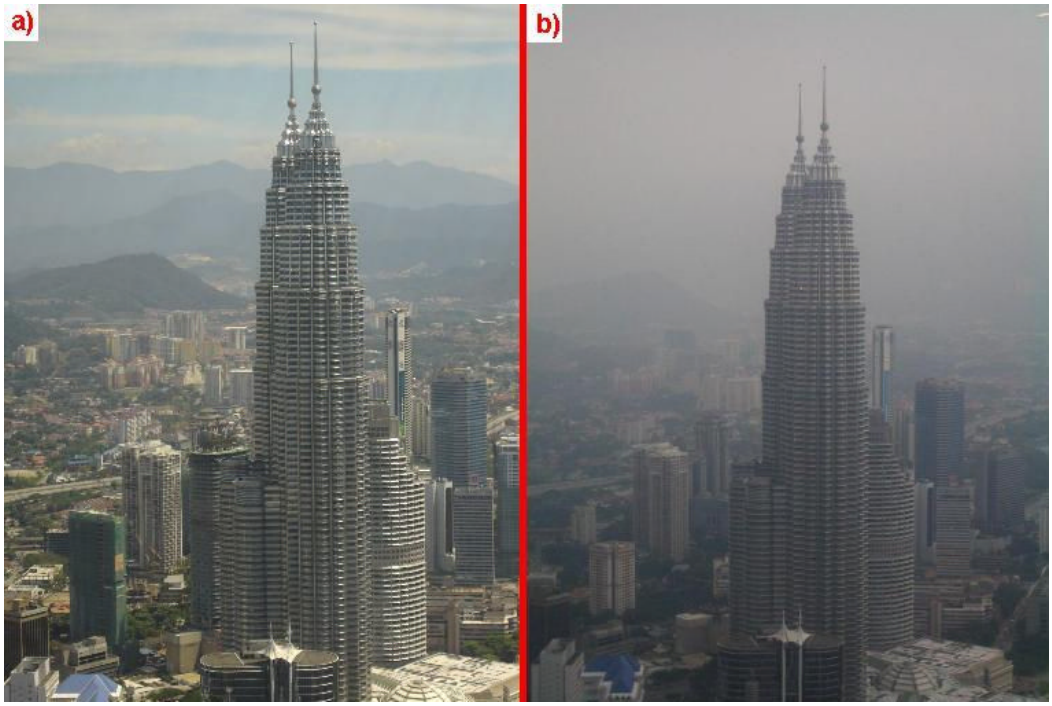

Figure 1.1. Effect of haze layers in visibility reduction: view of Petronas towers and the valley during a) a clear sunny day and b) during a haze episode. (Figure source: http://www.flickr.com/photos/khozem. Last checked on 15/02/2011)

Aerosols tend to affect the radiative balance of the climate system and affect the hydrological cycle [*Ramanathan et al.*, 2001; *Rosenfeld et al.*, 2008; *Satheesh and Ramanathan*, 2000] through the direct effect (scattering and absorbing of the incoming solar radiation) [*Ramanathan et al.*, 2001; *Schwartz*, 1996] and the indirect effect (acting as cloud condensation nuclei and hence changing the cloud cover, their albedo and life time) [*Lohmann and Feichter*, 2005]. Both effects have a net cooling effect on climate as opposed to a warming

effect exerted by greenhouse gases [*Charlson et al.*, 1992]. Radiative properties of aerosols are affected by their chemical composition, size distribution and ambient relative humidity (*RH*), thus making them highly variable both spatially and temporally. This induces large uncertainty in the estimation of the Earth's radiation budget. The radiative effects of aerosols can be quantified in terms of radiative forcing (ΔF). ΔF is defined by the *IPCC* [2007] as 'the change in net (down minus up) irradiance (solar plus longwave; in Wm^{-2}) at the tropopause after allowing for stratospheric temperatures to readjust to radiative equilibrium, but with surface and tropospheric temperatures and state held fixed at the unperturbed values'. ΔF and mean equilibrium surface temperature are linearly related [*Ramaswamy et al.*, 2001; *Seinfeld and Pandis*, 2006] which means that a negative ΔF indicates a global mean surface cooling and vice versa.

Figure 1.2, reprinted from the 4th Assessment Report on Climate Change (AR4) [*IPCC*, 2007] by the Intergovernmental Panel on Climate Change (IPCC), shows the magnitude of ΔF (values for the year 2005 relative to start of the industrialization ~ 1750) by different atmospheric components. ΔF for the greenhouse gases is positive with a high level of scientific understanding, given the long lifetime of greenhouse gases and their well understood production and removal processes. On the other hand, aerosols exert a cooling effect (negative ΔF) through their direct and indirect effects. Uncertainties associated with aerosol forcing are large because of the high temporal and spatial variability in aerosol physicochemical properties.

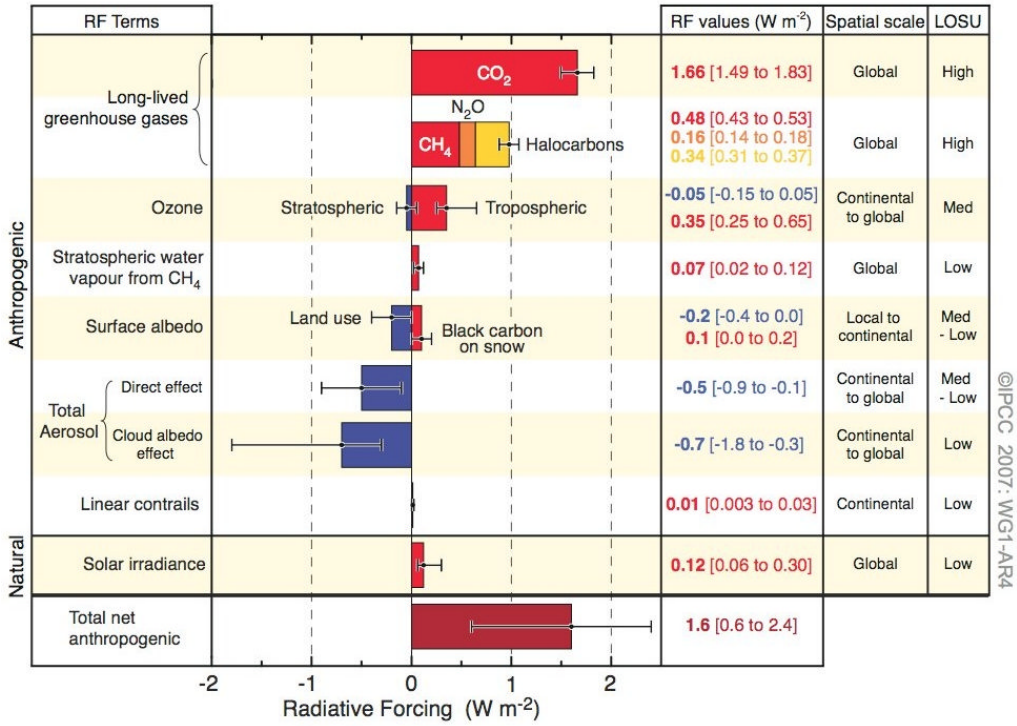

Figure 1.2. Radiative forcing due to anthropogenic and natural components and associated uncertainties, spatial scale and level of scientific understanding. Red colour indicates a positive forcing (warming effect) and blue colour a negative forcing (cooling effect). Forcing values are for the year 2005 relative to start of the industrialization (~ 1750). Reprinted from AR4 of IPCC, 2007.

1.1.1. Aerosol direct effect

Aerosols scatter and absorb incoming solar radiation thus increasing the albedo of the surface beneath. This leads to a net cooling effect on the surface and is a direct effect as it is an immediate effect exerted by aerosols on the climate. Aerosol chemical composition (which influences refractive index), aerosol size distribution and number concentration directly influence the magnitude of the direct aerosol radiative forcing. Water uptake by aerosol particles changes their chemical composition and size and hence their radiative properties [*Covert et al.*, 1972; *Tang*, 1996]. Hence radiative forcing strongly depends on the ambient *RH*. *Haywood and Shine* [1995] proposed the formulation (Eq. 1.1) for the quantification of Top of Atmosphere (*TOA*) aerosol radiative forcing (ΔF) for an optically thin partially absorbing aerosol layer:

$$\Delta F = -DS_0 T_{at}^2 (1 - A_c)\omega_0 \beta\delta\left[(1 - R_s)^2 - \left(2R_s/\beta\right)\left(\frac{1}{\omega_0} - 1\right)\right]$$

Eq. 1.1

where D is the fraction day length, S_0 is the solar constant, T_{at} is the atmospheric transmission, A_c is the fractional cloud cover, ω_0 is the RH dependent single scattering albedo, β is the RH dependent up-scatter fraction, δ is the RH dependent aerosol optical thickness, and R_s is the surface reflectance. β can be parameterized from the backscatter fraction (b) using the formulation of *Wiscombe and Grams* [1976].

The factors D, S_0, T_{at}, A_c and R_s can be treated as constant values. While D, S_0, T_{at} and A_c will only increase or decrease the magnitude of ΔF, R_s has the potential to reverse the sign of ΔF from positive to negative or vice versa and hence its accuracy is vital. R_s depends on the geographical location and the solar zenith angle and can have values between 0.03 and 1.0 [*Hummel and Reck*, 1979; *Robock*, 1980]. Water bodies have the largest span of R_s (0.03 – 1.0) depending upon solar zenith angle. For the North Atlantic summer, a value of R_s = 0.06, with the Sun at the zenith, is a good approximation [*Payne*, 1972].

The global average ΔF for aerosols is negative (i.e. net cooling effect) but individual aerosol species can have positive or negative ΔF values. For example, ΔF for biomass burning is +0.03 W m^{-2} and for fossil fuel black carbon it is +0.2 W m^{-2} whereas for sulphate, organic carbon and nitrate it is -0.4, -0.05 and -0.1 W m^{-2} respectively [*IPCC*, 2007]. ΔF changes sign from positive to negative (or vice versa) depending upon the critical value of the single scattering albedo (ω_{crit}) (Eq. 1.2). For $\omega_0 > \omega_{crit}$ there is a net cooling effect. The underlying surface along with aerosol chemical composition and size plays a crucial role in defining the sign of radiative forcing (negative or positive). Absorbing aerosols over a bright surface will result in a positive ΔF (warming effect) while more scattering aerosols over a dark surface will have a negative ΔF (cooling effect).

Haywood and Shine [1995] have detailed the values of ω_{crit} as a function of R_s at different β values.

$$\omega_{crit} = \frac{2R_s}{2R_s + \beta(1 - R_s)^2}$$

Eq. 1.2

1.1.2. Aerosol indirect effect

Aerosol particles act as seeds or so-called nuclei for the condensation of water and at critical super-saturation are activated as cloud droplets. Cloud condensation nuclei (CCN) is a term used for aerosol particles with a potential to become activated as cloud droplets if favourable conditions prevail. If there are no CCNs present, there will be no cloud formation. Clouds reflect the incoming solar radiation back to space and absorb the outgoing longwave radiation. Hence aerosols influence the radiative balance of the Earth system indirectly by changing cloud properties e.g. cloud lifetime and cloud albedo.

The first and most important indirect effect of aerosols is in increasing the albedo of the clouds. This is due to increased number concentration of CCN particles which reduce the net water content of the cloud droplets hence increasing the scattering associated with smaller droplets, leading to an increase in albedo [*Twomey*, 1977]. This effect is called the Twomey effect or cloud albedo effect. An excellent illustrative example of this effect is shown in Figure 1.3 (reprinted from *Johnson et al.*, 1996) which shows the ship tracks more reflective than the background cloud. These tracks are formed from the activation of ship stack aerosol emissions. Higher reflectivity of the tracks is due to an increase in cloud droplet number concentration leading to smaller sized droplets.

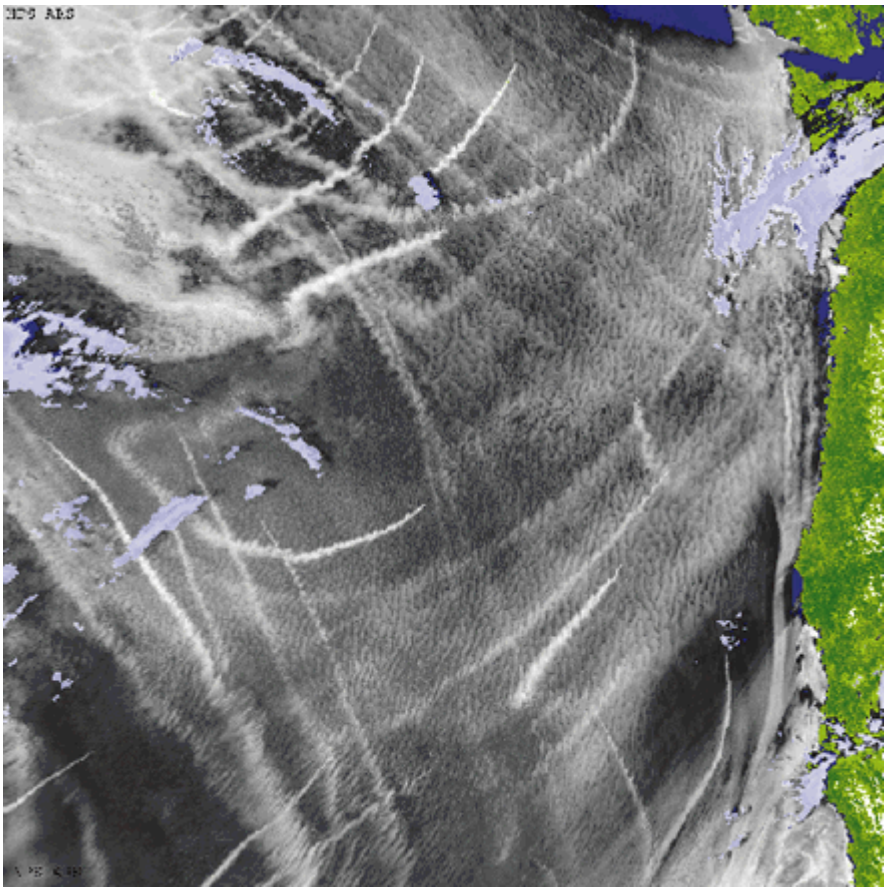

Figure 1.3. AVHRR satellite image of highly reflective ship tracks produced by ship stack emissions off the western coast of the United States. Reprinted from *Johnson et al.*, [1996].

The second indirect effect of aerosols influences the lifetime of clouds [*Albrecht*, 1989] and is also called the cloud lifetime effect or Albrecht effect. More numerous CCN will lead to smaller and more cloud droplets resulting in brighter clouds but also will reduce precipitation efficiency. The reduction in precipitation will increase the lifetime of clouds and, at times, their horizontal and vertical extent. This will further increase the cloud albedo and contributes to a cooling effect in addition to the Twomey effect.

There is also a semi-direct effect which results from carbonaceous aerosols in the cloud layer absorbing the incoming solar radiation thus heating the layer and reducing surface water vapour evaporation. This effect inhibits the cloud formation process.

A comprehensive review of indirect effect of aerosols is given by *Lohmann and Feichter* [2005].

1.2. Natural aerosols

Sea-spray, soil dust, volcanic ash and secondary aerosols from DMS account for the largest body of natural aerosols in the atmosphere. Natural aerosol emission budget estimates are approximately two orders of magnitude higher than the emission budget estimates of anthropogenic aerosols. There are far fewer studies of natural aerosols and their radiative impact on the climate as compared to anthropogenic aerosols, despite the importance of the former. Anthropogenic aerosols and greenhouse gases concentration is continuously increasing due to human activities (biomass / fossil fuel burning) thus increasing the global mean temperature. This may increase the global natural aerosol production in two ways: i) by increasing the arid land area due to a decrease in precipitation, and thus increasing the production of soil dust [*Woodward et al.*, 2005], and ii) by increasing the production of sea-spray aerosols due to higher wind-speeds accompanying warmer climate [*Latham and Smith*, 1990].

A major fraction of natural aerosols (sea-salt) is an efficient scatterer and is highly hygroscopic. Natural aerosol scattering particles partially offset the warming due to absorbing aerosols, both natural and anthropogenic, and due to greenhouse gases. Enhanced concentration of natural hygroscopic aerosols due to increasing global temperatures will lead to enhanced CCN number concentration, thus increasing the cloud albedo and further cooling the climate. Direct radiative impact of natural aerosols is generally small (with the exception of marine aerosols under conditions of moderately high to high wind speed conditions) compared to anthropogenic aerosols, but their indirect effect (and associated uncertainties) is much larger. Hence it is necessary to enhance our understanding of natural aerosols, their production mechanisms, and their radiative effects in a warming atmosphere.

1.2.1. Why study Marine aerosols?

The marine aerosol emission budget greatly surpasses any other source of natural or anthropogenic aerosol emission budget. This is due to the fact that approximately 70% of the Earth's surface is covered by the ocean. Given the fact that the ocean surface is dark (albedo ~ 0.06 [*Payne*, 1972]) and marine aerosols readily act as efficient CCN [*O'Dowd and Smith*, 1993; *O'Dowd et al.*, 1999a; *Ovadnevaite et al.*, 2011], cloud layers formed by, or modified by marine aerosols are likely to have a significant impact on the global radiative budget.

In the clean marine atmosphere two distinct aerosol types are present: i) primary produced sea-spray aerosol due to mechanical disruption of the ocean surface by wind, and ii) secondary aerosols: non-sea-salt (nss) sulphate and organics formed by gas-to-particle conversion processes. Sea-spray aerosol is one of the most significant natural aerosol components with global emissions of the order of 6297 Tg y^{-1} [*Vignati et al.*, 2010]. A recent review by *de Leeuw et al.*, [2011] points out large differences across a wider range of budget estimates of sea-spray. nss sulphate have emissions in the range 15 – 33 Tg S y^{-1} [*Kettle and Andreae*, 2000] and primary organics ~ 17.2 Tg y^{-1} [*Vignati et al.*, 2010].

Organic matter may contribute significantly, depending upon the ocean productivity, to the sub-µm sea-spray mass fraction [*O'Dowd et al.*, 2004]. Despite the fact that the primary organic matter associated with sea-spray is almost exclusively water insoluble [*Facchini et al.*, 2008], *Ovadnevaite et al.* [2011] found that water insoluble organic enriched sea-spray have almost a 100% activation efficiency even at a low supersaturation of 0.2%. Sea salt nuclei are preferred over sulphate nuclei for activation in marine clouds [*O'Dowd et al.*, 1999b]. Sea-spray is a dominant scatterer in the marine environment [*Kleefeld et al.*, 2002] and its mass flux is directly dependent on wind-speed through a power law [*Ovadnevaite et al.*, 2012]. Indeed, a high correlation coefficient of 0.97 was found between aerosol optical depth (*AOD*) and wind-speed [*Mulcahy et al.*, 2008] with *AOD* values of 0.3-0.4 at moderately high wind speed. AOD was also found to be dependent upon wind-speed through a power law. These findings points to a significant role for sea-spray in the direct radiative effect.

1.2.2. The Mace Head Atmospheric Research Station

The Mace Head Atmospheric Research Station (53^0 19'N, 9^0 54' W) is a World Meteorological Organization (WMO) – Global Atmosphere Watch (GAW) site strategically positioned on the west coast (near Carna, Co. Galway) of Ireland. The site is located 88km west from the nearest urban agglomeration of Galway City. Its unique location on the north-eastern edge of the Atlantic Ocean enables it to receive air masses of different origin and hence different aerosol type [*Jennings et al.*, 1991; 1997]. In approximately 50% of cases throughout the year, air masses arriving at the site are from the designated clean marine sector of 190^0-300^0 [*Jennings et al.*, 2003]. Table 1.1 summarizes the frequency of occurrence of black carbon (BC) mass concentration in clean (190^0-300^0), continental (45^0-135^0) and modified (300^0-0^0 - 45^0 & 135^0-190^0) wind sectors based on ten years (2001-2010) of meteorological and BC datasets. Figure 1.4 is the visual representation of Table 1.1.

Table 1.1. Percentage occurrence of BC mass concentration in clean marine, continental and modified wind sectors.

BC concentration (ng m^{-3})	Wind sector			Total
	190^0-300^0	45^0-135^0	300^0- 0^0 - 45^0 & 135^0-190^0	
	Percentage occurrence (%)			
BC <= 50	40.11	1.93	17.76	59.80
BC >= 150	3.04	13.85	5.69	22.58
50 < BC < 150	6.16	4.12	7.34	17.62
Total	49.31	19.90	30.79	100.00

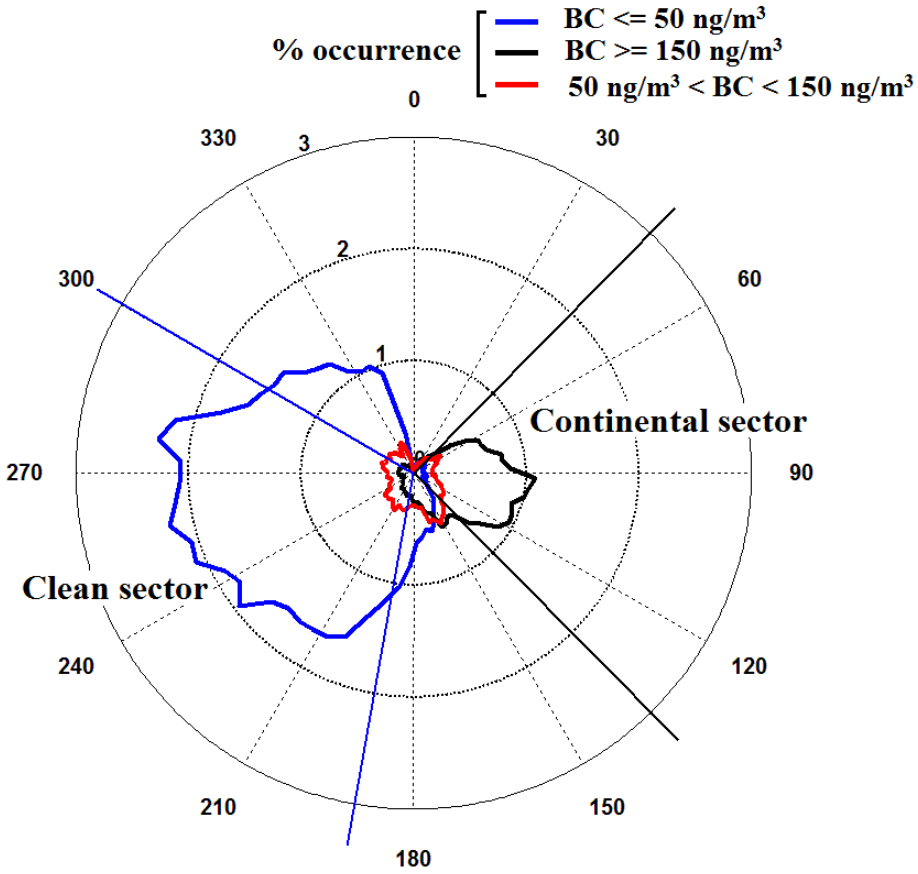

Figure 1.4. Percentage occurrence of BC concentration in clean marine, continental and modified wind sectors.

Maritime aerosols having air mass history of 4-6 days over the North Atlantic Ocean are likely to be dominated by $(NH_4)_2SO_4$ and *NaCl*, for particle radius <0.2 µm and >0.2 µm, respectively [*Jennings and O'Dowd*, 1990]. Also, the aged maritime air masses have high number concentration of coarse mode particles [*Jennings et al.*, 1991] indicating the dominance of sea-salt in the marine environment. Both $(NH_4)_2SO_4$ and *NaCl* are known to be highly hygroscopic [*Covert et al.*, 1972; *Tang*, 1976]. *O'Dowd et al.* [2004] reported high concentrations of organic matter in the sub-µm range during the spring to autumn season in ambient aerosols when air masses arriving at the research station were from the clean marine sector. The winter season is characterized by low biological activity (LBA) period in the North Atlantic Ocean in contrast to high biological activity (HBA) during the spring to autumn season, as shown in Figure 1.5A & 1.5B, respectively. O'Dowd et al., [2004] concluded that during the LBA period, organic matter contributes 15% to the sub-µm aerosol mass, in

contrast to 63% during the HBA period, as shown in Figure 1.5C and 1.5D, respectively.

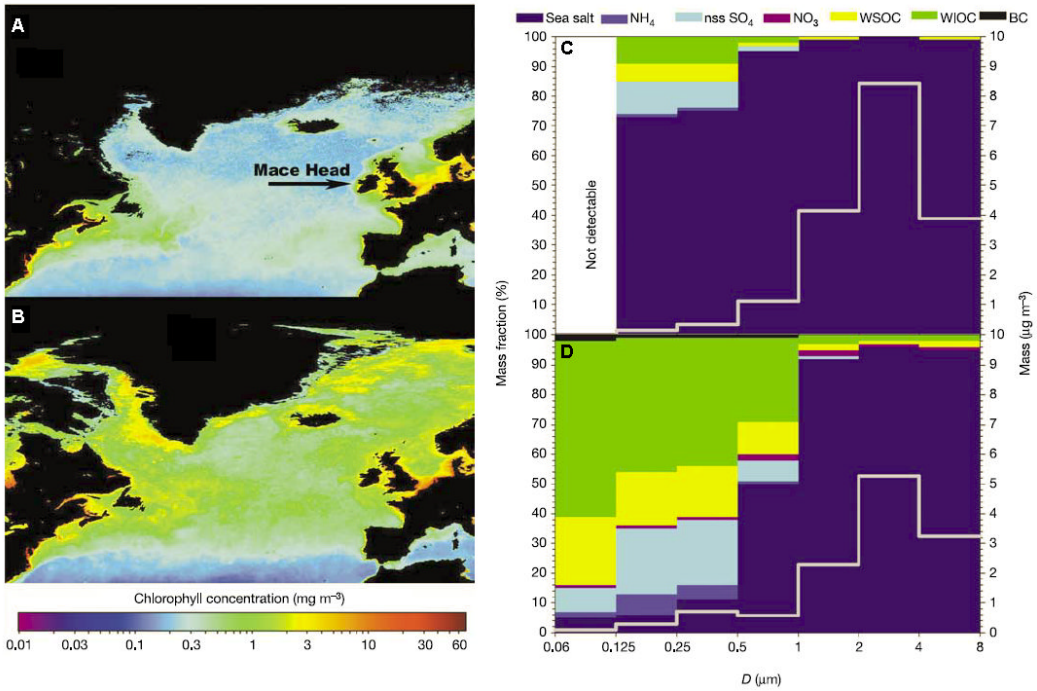

Figure 1.5. Left panel: SeaWiFS-derived seasonal average (5-year) sea-surface chlorophyll concentrations in winter (A) and spring (B), illustrating low biological activity in North Atlantic waters during winter and high biological activity in spring (courtesy of SeaWiFS Project, NASA/Goddard Space Flight Center and ORBIMAGE). Right panel: Average size-segregated chemical compositions and absolute mass concentrations for North Atlantic marine aerosols sampled with a Berner Impactor, for LBA (C) and HBA (D) periods. The concentrations of water soluble organic matter, water insoluble organic matter and black carbon are reported as mass of organic matter. Reprinted from O'Dowd et al., [2004].

Yoon et al. [2007] reported similar seasonal variations in the mass concentration of sea-salt, non-sea-salt (nss) sulphate, water soluble organic carbon (WSOC) and total carbon (TC). WSOC has a distinct seasonal pattern with mass concentration reaching 0.2 $\mu g\ C\ m^{-3}$ during the HBA period and 0.05 $\mu g\ C\ m^{-3}$ during the LBA period. While sea-salt mass concentration showed maxima in the winter season and minima in the summer season, nss sulphate mass concentration in the fine mode exhibited an opposite trend. Sea-salt aerosol production is directly linked with wind speed generated sea-spray [*Ovadnevaite et al.*, 2012] which is higher during the winter season in the North Atlantic Ocean. Super-µm particles contribute more to the aerosol light scattering

coefficient as compared to sub-μm particles over the North Atlantic Ocean [*Kleefeld et al.*, 2002] and this contribution is directly related to wind-speed (*U*) generated sea-salt particles. Direct evidence of this can be seen from the aerosol light scattering coefficient (σ_{scat}) values which exhibit a maximum (21 Mm^{-1}) in the winter season as compared to the summer season [*Yoon et al.*, 2007]. *Mulcahy et al.* [2008] reported that for clean marine air-masses over the North Atlantic Ocean, a high correlation of 0.97 between aerosol optical depth (*AOD*) and U^2 exists, thus confirming the contribution of sea-spray generated aerosols to enhanced σ_{scat} values during the winter season. A summary of the principal findings of research on aerosols carried out at the Mace Head Atmospheric Research Station during the last fifty years is presented by *O'Connor et al.* [2008].

1.3. Factors influencing the optical properties of marine aerosols

Long-term measurements of aerosol radiative properties are key for developing a better understanding of their climatic implications. Sea-spray aerosols act as efficient CCN [*O'Dowd et al.*, 1999b] and hence play a major role in defining the cloud cover and its properties in the pristine marine environment. Bright clouds over dark ocean surface have a cooling effect on the climate as they reflect significant portion of incoming solar radiation back to space which otherwise will be absorbed by the ocean. Production of sea-spray aerosols is driven by wind-speed [*O'Dowd and Smith*, 1993]. Sea-spray aerosol radiative properties are influenced by *RH* [*Tang et al.*, 1997] and ocean near-surface layer chemical composition which show a seasonal behaviour [*O'Dowd et al.*, 2004; *Yoon et al.*, 2007]. Hence it is important to examine the effects of wind-speed, *RH* and ocean near-surface chemical composition on the radiative properties of sea-spray aerosols in order to reduce uncertainties in the estimation of the Earth's radiation budget and to have more reliable climate predictions.

1.3.1. Wind speed

The sea-spray aerosol production mechanism is driven by wind-speed. Air entrained in the near surface layer of the ocean water, due to wind stress, rises quickly in the form of air bubbles and burst as they reach the surface water. The bursting of air bubbles causes production of film and jet drops [*Blanchard*, 1963; *Blanchard and Woodcock*, 1957]. The production of film and jet drops occur at wind speeds higher than 3 - 4 m s^{-1}. These bubble films when burst, due to pressure difference across the surface, form hundreds of sea-water drops which rapidly equilibrate to ambient *RH*, leaving behind sea-salt film droplets in the size range 0.1 – 1 μm [*Woodcock*, 1972; *Woolf et al.*, 1987]. The cavity, which remains after the film bursts, thus collapses due to instabilities leading to the formation of an upward movement of a water jet which fragments into a few jet-droplets with size range 1 – 10 μm [*Blanchard*, 1963]. At wind speeds in excess of 10 m s^{-1}, the tearing of wave crests results in the injection of spume droplets, typically in the size range 10 – 100 μm [*Jin*, 1993; *Wang and Street*, 1978]. The flux of sea-spray thus produced follows a power law dependency on wind speed [*O'Dowd et al.*, 1997].

In recent years, comprehensive reviews of sea-spray production have been reported [*de Leeuw et al.*, 2011; *Lewis and Schwartz*, 2004; *O'Dowd and de Leeuw*, 2007].

As sea-spray aerosol production increases with increasing wind speed, it contributes more to sub-μm and super-μm scattering [*Kleefeld et al.*, 2002; *Quinn et al.*, 1996]. This observation is supported by the finding of *Mulcahy et al.* [2008], where a square dependency on wind speed and columnar *AOD* has been reported. This influences incoming solar radiation by altering the cloud properties [*O'Dowd and Smith*, 1993; *O'Dowd et al.*, 1999a] and hence the radiative balance of the atmosphere [*Murphy et al.*, 1998].

1.3.2. Chemical composition and relative humidity

Changes in chemical composition of aerosol particles influences their complex refractive index and hence their light scattering properties. In other words, in order to study the chemical composition effect on aerosol light scattering one should study the effects of aerosol complex refractive index variations on light scattering by aerosols. *Jennings et al,.* [1978] have performed sensitivity analysis using Mie scattering theory [*Bohren and Huffman*, 1983] to determine the effect of variations in complex refractive index on volume extinction for a wide range of log-normal particle size distributions. *Horvath* [1993] presented a comprehensive review of absorbing aerosols (ie. aerosols with imaginary index of refraction).

RH is a key meteorological parameter which has a direct bearing on aerosol radiative properties [*Ramaswamy et al.*, 2001; *Rood et al.*, 1989]. The hygroscopicity of an aerosol particle is related to its chemical composition [*Covert et al.*, 1972] and mixing state (internal or external). WMO/GAW recommends measuring σ_{scat} at $RH < 40\%$ [*Baltensperger*, 2003] in order to enable comparison of results from different measuring stations. Further, it also gives emphasis to the measurement of σ_{scat} at ambient *RH* along with $RH < 40\%$ for stations that encounter a variety of aerosol types. Figure 1.6 illustrates the response of a hygroscopic aerosol particle as the *RH* increases from 40 % to > 75 %. As the size of the particle increases, due to water uptake at high *RH*, the surface area increases, hence increasing its scattering efficiency [*Tang*, 1996].

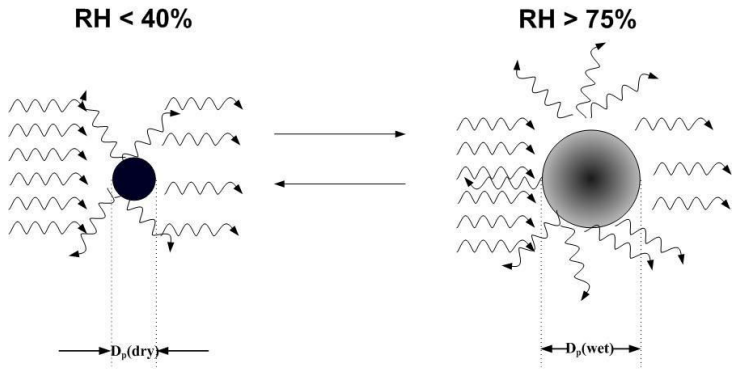

Figure 1.6. Increase in aerosol surface area due to increasing water uptake at higher relative humidity.

Figure 1.7 [*Rood et al.*, 1987a] illustrates the relative diameter change of different chemical compounds to change in *RH*. A hygroscopic compound with no deliquescent properties (Figure 1.7A) responds monotonously to changes in *RH* while hygroscopic compounds with deliquescent properties respond differently to increasing and decreasing *RH* (Figure 1.7B). A mixture of chemical compounds with different deliquescent points responds in a complex way to changes in *RH* (Figure 1.7C).

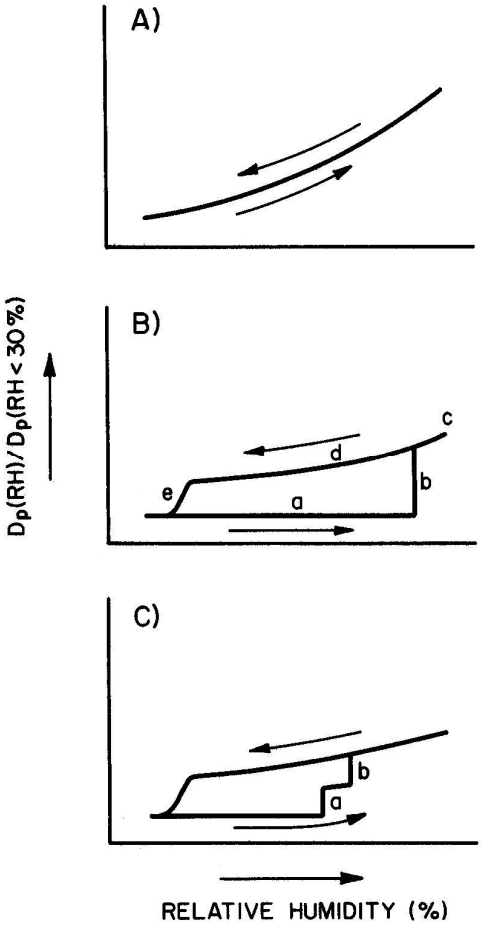

Figure 1.7. Aerosol particle size response as a function of *RH* for (A) a hygroscopic compound with no deliquescent properties, (B) a pure hygroscopic compound with deliquescent properties, and (C) a mixture of hygroscopic compounds with deliquescent properties. Reprinted from *Rood et al.*, [1987a].

The scattering enhancement factor ($f(RH,\lambda)$) describes the effect of *RH* on aerosol light scattering properties. $f(RH,\lambda)$ is an intensive optical property and is defined as the ratio of light scattering at high *RH* to that at low *RH* (Eq. 1.3).

$$f(RH,\lambda)=\frac{\sigma_{scat}^{\lambda}(RH)}{\sigma_{scat}^{\lambda}(RH<40\%)}$$

Eq. 1.3

f(RH,λ) can be calculated by measuring σ_{scat} at high *RH* and at low *RH*. This is achieved by operating two nephelometers [*Ahlquist and Charlson*, 1967] in series or in parallel, one measuring under dry (< 40 % *RH*) conditions and the other at high *RH*, generally more than 75 %. Because of the heat generated by the 75 watt lamp, the Nephelometer restricts the measurement of σ_{scat} to be performed at low *RH* only [*Anderson et al.*, 1996]. In order to overcome this problem, control and scan of *RH* upstream of the Nephelometer is essential and has been carried out previously. A compilation of major efforts towards realization of a scanning *RH* Nephelometer system (Humidograph) is presented in Table 1.2.

Table 1.2. Summary of work carried out by researchers towards realization of a humidification system.

Reference	Remark
[*Covert et al.*, 1972]	A chamber to mix water vapour and sample air (humidifier) upstream of the Nephelometer.
[*Rood et al.*, 1985]	Same as Covert et al., 1972, with additional heating and cooling assembly in between a humidifier and the Nephelometer to study the hysteresis behaviour of the aerosol particles.
[*Rood et al.*, 1987a; b]	Humidity and temperature controlled Nephelometer to study the effect of *RH* and temperature on hygroscopic properties of aerosol and to quantify the NH_4^+/SO_4^{2-} molar ratio and sulfate mass concentration.
[*Carrico*, 1995]	Development and automation of a controlled *RH* scanning aerosol system (Humidograph) using a Gore-Tex tube, for measuring aerosol σ_{scat}.
[*ten Brink et al.*, 2000]	A high flow humidograph system to test the hysteresis of water uptake of sub-micron aerosol particles.

[*Day and Malm*, 2001]	A humidograph system using a Perma Pure drying tube was constructed. By comparing the field data obtained from three rural National parks in the US and from filter samples, it was found that soluble inorganic material were much more hygroscopic than organic carbon and soil.
[*Kus et al.*, 2004]	Humidograph system along with measurement of particle hygroscopic growth and number concentration to enable comparison of measured and modeled *f(RH)*.
[*Fierz-Schmidhauser et al.*, 2010a]	*RH* dependent measurement of σ_{scat} using a Humidograph and studying the hysteresis effect. Comparison with results based on Mie theory using additional inputs (size distribution and number concentration).

Zieger [2011] has calculated the *f(RH, 550nm)*, using Mie scattering model, for aerosols listed in the optical properties of aerosols and clouds (OPAC) database [Hess et al., 1998] as shown in Figure 1.8. The highest *f(RH)* values are for aerosols pertaining to maritime and Arctic air masses as they are dominated by hygroscopic salt and sulphate compounds. The lowest *f(RH)* values are for desert dust aerosols.

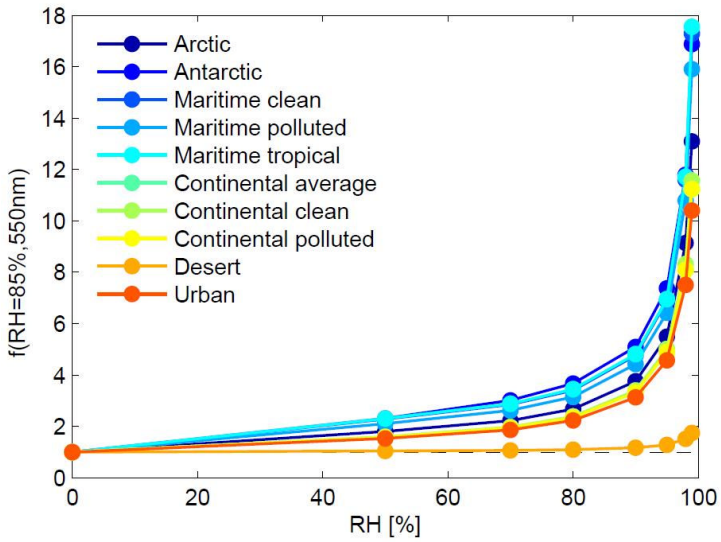

Figure 1.8. Scattering enhancement factors calculated for different model aerosol types. The OPAC database [*Hess et al.*, 1998] used here is given at eight discrete relative humidities. Reprinted from *Zieger* [2011].

A summary of aerosol light scattering enhancement factor *f(RH)* for different air mass types found worldwide during various field campaigns is given in Table 1.3.

Table 1.3. Reported studies on hygroscopicity of aerosols using a Humidograph system for different air-masses and locations.

***Air mass* type : location**	***f(RH)***	***RH (%)***	**Reference**
Urban : Seattle, Washington Altadena, California Denver, Colorado	2.00 2.50 ~1.40	85.0	[*Covert et al.*, 1972]
Urban: Seattle, Washington	~1.35	80.0	[*Rood et al.*, 1985]
Urban: Riverside, California	~1.76	63.6	[*Rood et al.*, 1987a]
Biomass burning: (Brazil) Cuiaba Porto Velho Maraba	1.07 1.10 1.32	80	[*Kotchenruther and Hobbs*, 1998]
Polluted Marine Sable Island, Canada	1.70 2.70	85.0	[*McInnes et al.*, 1998]
Western airflow (more anthropogenic) Northern airflow (less anthropogenic): Mid-Atlantic coast, US	2.30±0.24 1.81±0.37	80	[*Kotchenruther et al.*, 1999]
Rural: Grand Canyon Big Bend	2.51 2.58	87.6 87.5	[*Day and Malm*, 2001]
Anthropogenic: North Indian Ocean (INDOEX)	1.58±0.21	85	[*Sheridan et al.*, 2002]
Biomass burning: Yangtze Delta, China	1.70-2.00	80	[*Xu et al.*, 2002]
Marine Polluted Volcanic Dust ACE-Asia	2.95 2.52 2.61 2.10	82.0	[*Carrico et al.*, 2003]

Biomass burning (dry): Ambient air in Mozambique, Smoke plumes Botswana & Zambia	1.59±0.04 1.44±0.02	80	[*Magi and Hobbs*, 2003]
Dust Pollution (China) Pollution (Korea) Biomass East Asia (ACE-Asia)	2.00±0.27 2.75±0.38 1.91±0.16 1.60±0.20	85	[*Kim et al.*, 2006]
Urban Mixed Marine: PRD campaign,	2.04±0.28 2.29±0.28 2.68±0.29	80	[*Liu et al.*, 2008]
Polar: Zeppelin, Spitsbergen	3.24±0.63	85.0	[*Zieger et al.*, 2010]
Free Troposphere: Jungfraujoch, Switzerland	2.23	85.0	[*Fierz-Schmidhauser et al.*, 2010b]
Marine boundary layer: Clean marine Modified marine Mace Head, Ireland	2.22±0.17 1.77±0.31	85.0	[*Fierz-Schmidhauser et al.*, 2010c]

As mentioned in section 1.1, the uncertainties associated with aerosol forcing are large because of the high temporal and spatial variability in aerosol physicochemical properties. Long-term measurements of key aerosol properties at worldwide locations are effective in reducing the uncertainties associated with aerosol direct and indirect effects. For the North-Atlantic marine environment long-term measurements of aerosol scattering properties have not been reported previously and are therefore required to fill the knowledge-gap and to develop a better understanding of optical and physicochemical properties of aerosols. The dependency of aerosol light scattering properties on wind-speed, as described in section 1.3.1, is mostly studied and reported in terms of *AOD* [*Mulcahy et al.*, 2008; *Smirnov et al.*, 2003] and there have been few studies e.g., *Kleefeld et al.*, [2002] that have reported wind-dependent scattering coefficient dependency. Also, the information on seasonal variation on this dependency is lacking and hence need to be addressed. Other major factors which influence the aerosol light scattering properties are chemical composition and *RH*, as elaborated in section

1.3.2. In the North-Atlantic marine atmosphere, where air masses of different origin are frequently encountered, aerosol particles have diverse chemical composition. Enhanced biological activity in the ocean near-surface layer during the spring to summer months and higher wind-speeds during the winter months also contribute to diverse chemical composition exhibited by aerosols. Thus it is essential to study the scattering properties of aerosols in such dynamic marine environment.

During the literature review process a set of questions pertaining to marine aerosols were identified and are listed in the following section.

1.4. Questions addressed by the present study

Work done during the course of this PhD addresses the following questions pertaining to aerosols in the marine environment of the North-East Atlantic:

- Is there a seasonal pattern exhibited by aerosol scattering properties in the clean marine environment of the North-East Atlantic? If yes, then what are the driving forces behind the observed patterns?

- Can one quantify wind-driven influences on aerosol light scattering? How does sea-spray and ocean biota affect scattering magnitudes or their dependence on wind-speed in different seasons?

- How does relative humidity affect the light scattering properties of aerosols in clean and polluted marine environments?

- What role does aerosol chemical composition play in response of aerosols to changes in relative humidity? What are the radiative implications of this?

- What are the optical characteristics of ash cloud aerosols?

1.5. References

Ahlquist, N. C., and R. J. Charlson (1967), A new instrument for evaluating the visual quality of air, *J. Air Poll. Control Assoc.*, *17*(7), 467-469.

Albrecht, B. A. (1989), Aerosols, cloud microphysics, and fractional cloudiness, *Science*, *245*(4923), 1227-1230.

Anderson, T. L., et al. (1996), Performance characteristics of a high-sensitivity, three-wavelength, total scatter/backscatter nephelometer, *J. Atmos. Oceanic Technol.*, *13*(5), 967-986, doi: doi:10.1175/1520-0426(1996)013<0967%3APCOAHS>2.0.CO%3B2.

Andreae, M. O., and P. Merlet (2001), Emission of trace gases and aerosols from biomass burning, *G. Biogeochem. Cycl.*, *15*(4), 955-966, doi: 10.1029/2000gb001382.

Andreae, M. O., and D. Rosenfeld (2008), Aerosol-cloud-precipitation interactions. Part 1. The nature and sources of cloud-active aerosols, *Earth-Science Rev.*, *89*(1-2), 13-41, doi: 10.1016/j.earscirev.2008.03.001.

Baltensperger, U. (2003), WMO/GAW aerosol measurement procedures: Guidelines and recommendations, *WMO Tech. Doc*, *1178/153*, 72.

Blanchard, D. C. (1963), The electrification of the atmosphere by particles from bubbles in the sea, *Prog. Oceanog.*, *1*(C), 171-202.

Blanchard, D. C., and A. H. Woodcock (1957), Bubble formation and modification in the sea and its meteorological significance, *Tellus*, *9*(2), 145-158.

Bohren, C. F., and D. R. Huffman (1983), *Absorption and scattering of light by small particles*Ser., vol., J Wiley & Sons, New York.

Carrico, C. M. (1995), An automated, controlled relative humidity Nephelometer system for laboratory and ambient aerosol measurements, Master of Science thesis, 126 pp, University of Illinois, Illinois.

Carrico, C. M., P. Kus, M. J. Rood, P. K. Quinn, and T. S. Bates (2003), Mixtures of pollution, dust, sea salt, and volcanic aerosol during ACE-Asia: Radiative properties as a function of relative humidity, *J. Geophys. Res.*, *108*(D23), doi: 10.1029/2003JD003405.

Charlson, R. J., S. E. Schwartz, J. M. Hales, R. D. Cess, J. A. Coakley Jr, J. E. Hansen, and D. J. Hofmann (1992), Climate forcing by anthropogenic aerosols, *Science*, *255*(5043), 423-430.

Cofala, J., M. Amann, Z. Klimont, K. Kupiainen, and L. Höglund-Isaksson (2007), Scenarios of global anthropogenic emissions of air pollutants and methane until 2030, *Atmos. Environ.*, *41*(38), 8486-8499, doi: 10.1016/j.atmosenv.2007.07.010.

Covert, D. S., R. J. Charlson, and N. C. Ahlquist (1972), A Study of the Relationship of Chemical Composition and Humidity to Light Scattering by Aerosols, *J. Appl. Met.*, *11*(6), 968-976, doi: 10.1175/1520-0450(1972)011<0968%3AASOTRO>2.0.CO%3B2.

Day, D. E., and W. C. Malm (2001), Aerosol light scattering measurements as a function of relative humidity: A comparison between measurements made at three different sites, *Atmos. Environ.*, *35*(30), 5169-5176.

de Leeuw, G., E. L. Andreas, M. D. Anguelova, C. W. Fairall, E. R. Lewis, C. O'Dowd, M. Schulz, and S. E. Schwartz (2011), Production flux of sea spray aerosol, *Rev. Geophy.*, *49*(2), doi: 10.1029/2010rg000349.

Dentener, F., et al. (2006), Emissions of primary aerosol and precursor gases in the years 2000 and 1750 prescribed data-sets for AeroCom, *Atmos. Chem. Phys.*, *6*(12), 4321-4344, doi: 10.1029/2003.

Facchini, M. C., et al. (2008), Primary submicron marine aerosol dominated by insoluble organic colloids and aggregates, *Geophys. Res. Lett.*, *35*(17), doi: 10.1029/2008gl034210.

Fierz-Schmidhauser, R., P. Zieger, G. Wehrle, A. Jefferson, J. A. Ogren, U. Baltensperger, and E. Weingartner (2010a), Measurement of relative humidity dependent light scattering of aerosols, *Atmos. Meas. Tech.*, *3*(1), 39-50, doi: 10.1029/2003JD003405.

Fierz-Schmidhauser, R., P. Zieger, M. Gysel, L. Kammermann, P. F. DeCarlo, U. Baltensperger, and E. Weingartner (2010b), Measured and predicted aerosol light scattering enhancementfactors at the high alpine site Jungfraujoch, *Atmos. Chem. Phys.*, *10*(5), 2319-2333, doi: 10.1029/2003JD003405.

Fierz-Schmidhauser, R., P. Zieger, A. Vaishya, C. Monahan, J. Bialek, C. D. O'Dowd, S. G. Jennings, U. Baltensperger, and E. Weingartner (2010c), Light scattering enhancement factors in the marine boundary layer (Mace Head, Ireland), *J. Geophys. Res.*, *115*(20), D20204, doi: 10.1029/2009JD013755.

Haywood, J. M., and K. P. Shine (1995), The effect of anthropogenic sulfate and soot aerosol on the clear sky planetary radiation budget, *Geophys. Res. Lett.*, *22*(5), 603-606.

Hess, M., P. Koepke, and I. Schult (1998), Optical Properties of Aerosols and Clouds: The Software Package OPAC, *Bull. Ame. Met. Soc.*, *79*(5), 831-844.

Horvath, H. (1993), Atmospheric light absorption - A review, *Atmos. Environ.*, *27 A*(3), 293-317.

Hummel, J. R., and R. A. Reck (1979), A global surface albedo model, *J. Appl. Met.*, *18*(3), 239-253.

IPCC (2007), *The Physical Science Basis: Contribution of Working Group I to the Fourth Assessment Report of the Intergovernmental Panel on Climate Change*Ser., vol. 996, Cambridge University Press, Cambridge, United Kingdom and New York, NY, USA.

Jennings, S. G., and C. D. O'Dowd (1990), Volatility of aerosol at Mace Head, on the west coast of Ireland, *J. Geophys. Res.*, *95*(D9), 13,937-913,948, doi: doi:10.1029/JD095iD09p13937.

Jennings, S. G., R. G. Pinnick, and H. J. Auvermann (1978), Effects of particulate complex refractive index and particle size distribution variations on atmospheric extinction and absorption for visible through middle ir wavelengths, *Appl. Opt.*, *17*(24), 3922-3929.

Jennings, S. G., C. D. O'Dowd, T. C. O'Connor, and F. M. McGovern (1991), Physical characteristics of the ambient aerosol at Mace Head, *Atmos. Environ.*, *25 A*(3-4), 557-562.

Jennings, S. G., M. Geever, F. M. McGovern, J. Francis, T. G. Spain, and T. Donaghy (1997), Microphysical and physico-chemical characterization of

atmospheric marine and continental aerosol at Mace Head, *Atmos. Environ.*, *31*(17), 2795-2808.

Jennings, S. G., C. Kleefeld, C. D. O'Dowd, C. Junker, T. G. Spain, P. O'Brien, A. F. Roddy, and T. C. O'Connor (2003), Mace Head Atmospheric Research Station - Characterization of aerosol radiative parameters, *Boreal Environ. Res.*, *8*(4), 303-314.

Jin, W. (1993), Production of spume drops by the wind tearing of wave crests: the search for quantification, *J. Geophys. Res.*, *98*(C10), 18,221-218,227.

Johnson, D. W., S. R. Osborne, and J. P. Taylor (1996), The effects of a localised aerosol perturbation on the microphysics of a stratocumulus cloud layer, paper presented at The Fourteenth International Conference on Nucleation and Atmospheric Aerosols, Pergamon, Helsinki, 26 - 30 August.

Kettle, A. J., and M. O. Andreae (2000), Flux of dimethylsulfide from the oceans: A comparison of updated data sets and flux models, *J. Geophys. Res.*, *105*(D22), 26793-26808.

Kettle, A. J., et al. (1999), A global database of sea surface dimethylsulfide (DMS) measurements and a procedure to predict sea surface DMS as a function of latitude, longitude, and month, *G. Biogeochem. Cycl.*, *13*(2), 399-444.

Kim, J., S. C. Yoon, A. Jefferson, and S. W. Kim (2006), Aerosol hygroscopic properties during Asian dust, pollution, and biomass burning episodes at Gosan, Korea in April 2001, *Atmos. Environ.*, *40*(8), 1550-1560.

Kleefeld, C., C. D. O'Dowd, S. O'Reilly, S. G. Jennings, P. Aalto, E. Becker, G. Kunz, and G. De Leeuw (2002), Relative contribution of submicron and supermicron particles to aerosol light scattering in the marine boundary layer, *J. Geophys. Res.*, *107*(D19), doi: 10.1029/2000JD000262.

Kotchenruther, R. A., and P. V. Hobbs (1998), Humidification factors of aerosols from biomass burning in Brazil, *J. Geophys. Res.*, *103*(D24), 32081-32089.

Kotchenruther, R. A., P. V. Hobbs, and D. A. Hegg (1999), Humidification factors for atmospheric aerosols off the mid-Atlantic coast of the United States, *J. Geophys. Res.*, *104*(D2), 2239-2251.

Kus, P., C. M. Carrico, M. J. Rood, and A. Williams (2004), Measured and Modeled Light Scattering Values for Dry and Hydrated Laboratory Aerosols, *Journal of Atmospheric and Oceanic Technology*, *21*(7), 981-994.

Latham, J., and M. H. Smith (1990), Effect on global warming of wind-dependent aerosol generation at the ocean surface, *Nature*, *347*(6291), 372-373.

Lewis, E. R., and S. E. Schwartz (2004), *Sea salt aerosol production: mechanisms, methods, measurements and models: a critical review*,*Geophys. Monogr.* Ser., vol. 152, 413 pp., AGU, Washington, DC.

Liu, X., Y. Cheng, Y. Zhang, J. Jung, N. Sugimoto, S. y. Chang, Y. J. Kim, S. Fan, and L. Zeng (2008), Influences of relative humidity and particle chemical composition on aerosol scattering properties during the 2006 PRD campaign, *Atmos. Environ.*, *42*(7), 1525-1536.

Lohmann, U., and J. Feichter (2005), Global indirect aerosol effects: A review, *Atmos. Chem. Phys.*, *5*(3), 715-737.

Magi, B. I., and P. V. Hobbs (2003), Effects of humidity on aerosols in southern Africa during the biomass burning season, *J. Geophys. Res.*, *108*, D13.

McInnes, L., M. Bergin, J. Ogren, and S. Schwartz (1998), Apportionment of light scattering and hygroscopic growth to aerosol composition, *Geophys. Res. Lett.*, *25*(4), 513-516.

Mulcahy, J. P., C. D. O'Dowd, S. G. Jennings, and D. Ceburnis (2008), Significant enhancement of aerosol optical depth in marine air under high wind conditions, *Geophys. Res. Lett.*, *35*(16), L16810, doi: 10.1029/2008GL034303.

Murphy, D. M., J. R. Anderson, P. K. Qulnn, L. M. McLnnes, F. J. Brechtel, S. M. Kreidenwels, A. M. Middlebrook, M. PÃ³sfai, D. S. Thomson, and P. R. Buseck (1998), Influence of sea-salt on aerosol radiative properties in the Southern Ocean marine boundary layer, *Nature*, *392*(6671), 62-65, doi: DOI: 10.1038/32138.

O'Connor, T. C., S. G. Jennings, and C. D. O'Dowd (2008), Highlights of fifty years of atmospheric aerosol research at Mace Head, *Atmos. Res.*, *90*(2-4), 338-355, doi: 10.1016/j.atmosres.2008.08.014.

O'Dowd, C. D., and M. H. Smith (1993), Physicochemical properties of aerosols over the northeast Atlantic: evidence for wind-speed-related submicron sea-salt aerosol production, *J. Geophys. Res.*, *98*(D1), 1137-1149, doi: 10.1029/92JD02302.

O'Dowd, C. D., and G. de Leeuw (2007), Marine aerosol production: A review of the current knowledge, *Philosophical Transactions of the Royal Society A: Mathematical, Physical and Engineering Sciences*, *365*(1856), 1753-1774, doi: doi:10.1098/rsta.2007.2043.

O'Dowd, C. D., J. A. Lowe, and M. H. Smith (1999a), Coupling sea-salt and sulphate interactions and its impact on cloud droplet concentration predictions, *Geophysical Research Letters*, *26*(9), 1311-1314.

O'Dowd, C. D., M. H. Smith, I. E. Consterdine, and J. A. Lowe (1997), Marine aerosol, sea-salt, and the marine sulphur cycle: A short review, *Atmos. Environ.*, *31*(1), 73-80.

O'Dowd, C. D., J. A. Lowe, M. H. Smith, and A. D. Kaye (1999b), The relative importance of non-sea-salt sulphate and sea-salt aerosol to the marine cloud condensation nuclei population: An improved multi-component aerosol-cloud droplet parametrization, *Quart. J. of the Roy. Meteorol. Soc.*, *125*(556), 1295-1313.

O'Dowd, C. D., M. C. Facchini, F. Cavalli, D. Ceburnis, M. Mircea, S. Decesari, S. Fuzzi, J. Y. Young, and J. P. Putaud (2004), Biogenically driven organic contribution to marine aerosol, *Nature*, *431*(7009), 676-680, doi: 10.1038/nature02959.

Ovadnevaite, J., D. Ceburnis, M. Canagaratna, H. Berresheim, J. Bialek, D. R. Worsnop, and C. O'Dowd (2012), New findings on the effect of wind speed on submicron sea salt mass concentrations and source fluxes *J. Geophys. Res.*, Accepted manuscript.

Ovadnevaite, J., D. Ceburnis, G. Martucci, J. Bialek, C. Monahan, M. Rinaldi, M. C. Facchini, H. Berresheim, D. R. Worsnop, and C. O'Dowd (2011), Primary marine organic aerosol: A dichotomy of low hygroscopicity and high CCN activity, *Geophys. Res. Lett.*, *38*(21), L21806, doi: 10.1029/2011gl048869.

Payne, R. E. (1972), Albedo of the sea surface, *J. Atmos. Sci.*, *29*, 959-970.

Penner, J. E., C. C. Chuang, and K. Grant (1998), Climate forcing by carbonaceous and sulfate aerosols, *Climate Dynamics*, *14*(12), 839-851, doi: 10.1007/s003820050259.

Prospero, J. M. (1983), The atmospheric aerosol system: an overview, *Rev. Geophy. Space Phys.*, *21*(7), 1607-1629.

Quinn, P. K., V. N. Kapustin, T. S. Bates, and D. S. Covert (1996), Chemical and optical properties of marine boundary layer aerosol particles of the mid-Pacific in relation to sources and meteorological transport, *J. Geophys. Res.*, *101*(D3), 6931-6951.

Ramanathan, V., P. J. Crutzen, J. T. Kiehl, and D. Rosenfeld (2001), Atmosphere: Aerosols, climate, and the hydrological cycle, *Science*, *294*(5549), 2119-2124.

Ramaswamy, V., et al. (2001), Radiative forcing of climate change In: Climate Change 2001: The Scientific Basis. Contribution of Working Group I to the Third Assessment Report of the Intergovernmental Panel on Climate Change [Houghton, J.T.,Y. Ding, D.J. Griggs, M. Noguer, P.J. van der Linden, X. Dai, K. Maskell, and C.A. Johnson (eds.)], edited, Cambridge University Press, Cambridge, UK.

Robock, A. (1980), The seasonal cycle of snow cover, sea ice and surface albedo, *Monthly Weather Review*, *108*(3), 267-285.

Robock, A. (2000), Volcanic eruptions and climate, *Rev. Geophys.*, *38*(2), 191-219, doi: 10.1029/1998rg000054.

Rood, M. J., D. S. Covert, and T. V. Larson (1987a), Hygroscopic properties of atmospheric aerosol in Riverside, California, *Tellus, Ser. B*, *39 B*(4), 383-397.

Rood, M. J., D. S. Covert, and T. V. Larson (1987b), Temperature and humidity controlled nephelometry: Improvements and calibration, *Aerosol Sci. Technol.*, *7*(1), 57-65.

Rood, M. J., T. V. Larson, D. S. Covert, and N. C. Ahlquist (1985), Measurement of laboratory and ambient aerosols with temperature and humidity controlled nephelometry, *Atmos. Environ.*, *19*(7), 1181-1190.

Rood, M. J., M. A. Shaw, T. V. Larson, and D. S. Covert (1989), Ubiquitous nature of ambient metastable aerosol, *Nature*, *337*(6207), 537-539.

Rosenfeld, D., U. Lohmann, G. B. Raga, C. D. O'Dowd, M. Kulmala, S. Fuzzi, A. Reissell, and M. O. Andreae (2008), Flood or drought: How do aerosols affect precipitation?, *Science*, *321*(5894), 1309-1313, doi: 10.1126/science.1160606.

Satheesh, S. K., and V. Ramanathan (2000), Large differences in tropical aerosol forcing at the top of the atmosphere and Earth's surface, *Nature*, *405*(6782), 60-63.

Schwartz, S. E. (1996), The Whitehouse effect - Shortwave radiative forcing of climate by anthropogenic aerosols: An overview, *J. Aerosol Sci.*, *27*(3), 359-382.

Seinfeld, J. H., and S. N. Pandis (Eds.) (2006), *Atmospheric Chemistry and Physics: From air pollution to climate change*, 2nd ed., John Wiley & Sons, New York.

Sheridan, P. J., A. Jefferson, and J. A. Ogren (2002), Spatial variability of submicrometer aerosol radiative properties over the Indian Ocean during INDOEX, *J. Geophys. Res.*, *107*(D19).

Smirnov, A., B. N. Holben, T. F. Eck, O. Dubovik, and I. Slutsker (2003), Effect of wind speed on columnar aerosol optical properties at Midway Island, *J. Geophys. Res.*, *108*(D24), AAC 15-11 - AAC 15-18.

Tang, I. N. (1976), Phase transformation and growth of aerosol particles composed of mixed salts, *J. Aerosol Sci.*, *7*(5), 361-371.

Tang, I. N. (1996), Chemical and size effects of hygroscopic aerosols on light scattering coefficients, *J. Geophys. Res.*, *101*(14), 19,245-219,250, doi: 10.1029/96JD03003.

Tang, I. N., A. C. Tridico, and K. H. Fung (1997), Thermodynamic and optical properties of sea salt aerosols, *J. Geophys. Res.*, *102*(19), 23,269-223,275.

ten Brink, H. M., A. Khlystov, P. A. K. Gerard, T. Tuch, C. Roth, and W. Kreyling (2000), A high-flow humidograph for testing the water uptake by ambient aerosol, *Atmos. Environ.*, *34*(25), 4291-4300.

Twomey, S. (1977), The influence of pollution on the shortwave albedo of clouds, *J. Atmos. Sci.*, *34*, 1149-1152.

Vignati, E., M. C. Facchini, M. Rinaldi, C. Scannell, D. Ceburnis, J. Sciare, M. Kanakidou, S. Myriokefalitakis, F. Dentener, and C. D. O'Dowd (2010), Global scale emission and distribution of sea-spray aerosol: Sea-salt and organic enrichment, *Atmos. Environ.*, *44*(5), 670-677, doi: 10.1016/j.atmosenv.2009.11.013.

Wang, C. S., and R. L. Street (1978), Measurements of spray at an air-water interface, *Dyn. Atmos. Oceans*, *2*(2), 141-152.

Whitby, K. T. (1978), The physical characteristics of sulfur aerosols, *Atmos. Environ.*, *12*(1-3), 135-159.

Wiscombe, W. J., and G. W. Grams (1976), The backscattered fraction in two-stream approximations, *J. Atmos. Sci.*, *33*(12), 2440-2451.

Woodcock, A. H. (1972), Smaller salt particles in oceanic air and bubble behavior in the sea, *J. Geophys. Res.*, *77*(27), 5316-5321.

Woodward, S., D. L. Roberts, and R. A. Betts (2005), A simulation of the effect of climate change-induced desertification on mineral dust aerosol, *Geophys. Res. Lett.*, *32*(18), 1-4, doi: 10.1029/2005gl023482.

Woolf, D. K., P. A. Bowyer, and E. C. Monahan (1987), Discriminating between the film drops and jet drops produced by a simulated whitecap, *J. Geophys. Res.*, *92*(C5), 5142-5150.

Xu, J., M. H. Bergin, X. Yu, G. Liu, J. Zhao, C. M. Carrico, and K. Baumann (2002), Measurement of aerosol chemical, physical and radiative properties in the Yangtze delta region of China, *Atmos. Environ.*, *36*(2), 161-173.

Yoon, Y. J., et al. (2007), Seasonal characteristics of the physicochemical properties of North Atlantic marine atmospheric aerosols, *J. Geophys. Res.*, *112*(D4), D04206, doi: 10.1029/2005JD007044.

Zieger, P. (2011), Effects of relative humidity on aerosol light scattering, Ph.D. thesis, 152 pp, ETH Zurich, Switzerland.

Zieger, P., R. Fierz-Schmidhauser, M. Gysel, J. Strïm, S. Henne, K. E. Yttri, U. Baltensperger, and E. Weingartner (2010), Effects of relative humidity on aerosol light scattering in the Arctic, *Atmos. Chem. Phys.*, *10*(8), 3875-3890, doi: 10.1029/2003JD003405.

2. Summary of Research Papers

The work presented in this thesis consists of five peer-reviewed papers and one paper submitted for publication. In three of the papers I have a lead author role. One paper contains a major contribution from the candidate and two with minor contributions from the candidate.

Paper 1: Lead author

Seasonal variation of the aerosol light scattering coefficient in marine air of the Northeast Atlantic

Vaishya A., S.G. Jennings, C. O'Dowd (2011), *Adv. Meteorol.*, *vol. 2011*, Article ID 170490, doi:10.1155/2011/170490.

This paper presents a seasonal analysis of the aerosol light scattering properties, aerosol light scattering coefficient (σ_{scat}) and Ångström exponent ($\mathring{A}$), for clean marine air masses. Analysis presented is based on ten years (2001-2010) of aerosol light scattering measurements carried out using a TSI 3563 Integrating Nephelometer at the Mace Head Atmospheric Research Station. A wind-speed driven seasonal trend in σ_{scat} was observed, with σ_{scat} values reaching a maximum of ~ 35 Mm^{-1} in the month of January and a minimum of ~ 17 Mm^{-1} in the month of July. A high positive correlation coefficient of 0.88 was found between wind-speed and σ_{scat} while $\mathring{A}$ and wind-speed showed a negative correlation coefficient of -0.89. There also exists a high positive correlation between low $\mathring{A}$ and high σ_{scat} values thus indicating that wind-speed driven sea-spray contributed most to aerosol scattering during the winter season. In the summer season, when wind-speed shows a minimum for the year, non-sea-salt (nss) sulphate and organics are expected to contribute significantly to aerosol scattering. ***The author was responsible for the light scattering measurements (from 2008-2010), harmonizing ten years of light scattering, light absorption***

and meteorological datasets used in this study, its analysis, and the writing of the manuscript.

Paper 2: Lead author

Wind-driven influences on aerosol light scattering in North-East Atlantic air

Vaishya A., S.G. Jennings, C. O'Dowd (2012), *Geophy. Res. Lett.*, 39, L05805, doi:10.1029/2011GL050556.

This study quantified the influence of wind-speed (U) on aerosol light scattering using ten years (2001-2010) of aerosol light scattering measurements carried out at the Mace Head Atmsopheric Research Station. Both σ_{scat} and σ_{bscat} were found to be dependent on $\sim U^2$ with a high correlation coefficient of ~ 0.95. This dependency of σ_{scat} and σ_{bscat} on U holds true for both the winter (low biological activity - LBA) and for the summer (high biological activity - HBA) seasons. Ångström exponent (α) values revealed dominance of a super-µm mode in the LBA-period. LBA-period radiative values, σ_{scat} and σ_{bscat}, are approximately twice those of the HBA-period. Mie modelling studies, using real size distribution data for the LBA and the HBA periods, suggest that size distribution and refractive index (influenced by chemical composition) are key parameters accounting for 96% of observed differences in σ_{scat} and σ_{bscat}. Refractive index on its own accounted for 70% of the difference. ***The author was responsible for the light scattering measurements (from 2008-2010), harmonizing ten years of light scattering and meteorological datasets used in this study, its scientific analysis, and the writing of the manuscript.***

Paper 3: Contributing author: a major role

Light scattering enhancement factors in the marine boundary layer (Mace Head, Ireland)

Fierz-Schmidhauser R., P. Zieger, **A. Vaishya**, C. Monahan, J. Bialek, C.D. O'Dowd, S.G. Jennings, U. Baltensperger, E. Weingartner (2010), *J. Geophys. Res.*, 115 (20), D20204, doi:10.1029/2009JD013755.

This paper present the results of aerosol light scattering properties measured during a month long field campaign (January – February, 2009), at the Mace Head Atmospheric Research Station. A Wet-Nephelometer instrument (from Paul Scherrer Institute – PSI, Switzerland) was deployed to measure relative humidity (*RH*) dependent aerosol light scattering enhancement (*f(RH)*). Two major air mass types were identified: clean marine and modified (polluted) marine. *f*(85%, 550nm) values were 2.22 and 1.77 for clean and polluted air masses, respectively. Clean marine air masses showed a hysteresis behaviour in *f(RH)* with *f(55%)* values 35% higher for the dehydration branch as compared to the hydration branch. Polluted air masses showed no significant hysteresis effects. The measured values of *f(RH)* agree well with the Mie scattering model using size distribution and hygroscopic growth factor as inputs. Single scattering albedo (ω_0) was high with an average value of 0.99 for clean marine air masses and 0.89 for polluted air masses. ω_0 increased by ~ 5% for polluted air mass at 85% *RH*. The backscatter fraction remained between 0.10 and 0.12 for clean and polluted air masses and decreased by ~ 20% at 85% *RH* as compared to dry conditions. ***The author was responsible for all of the light scattering and the light absorption measurements, processing of dry light scattering and light absorption data, scientific analysis, and contributed partially to writing the manuscript.***

Paper 4: Lead author

Warming or cooling? The flippant effect of organics on sea-spray light-scattering

Vaishya A., J. Ovadnevaite, J. Bialek, S.G. Jennings, D. Ceburnis, C. O'Dowd, Submitted to *Nature Geoscience*.

This paper describes the effect of marine organics on aerosol hygroscopic and light scattering properties and its impact on the radiative cooling due to sea-spray aerosols. It was found that sea-spray *f(RH)* is suppressed by a factor of three when enriched with organic matter. This is due to the hydrophobic nature of primary organic material which suppresses the growth of sea-spray aerosol, and therefore reducing its light scattering ability at higher *RH*. A new hygroscopic growth-factor (*HGF*) parameterization for sea-spray was developed and presented as part of this study. This parameterization revealed a dual-hygroscopic state of sea-spray aerosol, flipping from high-hygroscopicity and high-*f(RH)* to low-hygroscopicity and low-*f(RH)* as the organic matter mixing volume percentage exceeds ~ 50%. This results in suppression of Top of Atmosphere (*TOA*) direct radiative forcing (ΔF) of sea-spray by ~ 4.5 times compared to pure sea-salt spray. These findings indicate a significant coupling between the marine biosphere and the direct radiative budget through alteration of sea-spray chemical composition. This could potentially lead to accelerated global warming, should biological activity increase with future projected temperature increases. ***The author developed the state-of-the-art scattering Humidograph instrument and collected, processed and analysed all related data, performed radiative forcing calculations and contributed to writing part of the manuscript and is lead author.***

Paper 5 : Contributing author: minor role

The Eyjafjallajökull ash plume Part I: Physical, chemical and optical characteristics

O'Dowd C.D., D. Ceburnis, J. Ovadnevaite, G. Martucci, J. Bialek, C. Monahan, H. Berresheim, **A. Vaishya**, T. Grigas, S.G. Jennings, P. McVeigh , S. Varghese, R. Flanagan, D. Martin, E. Moran, K. Lambkin, T. Semmler, C. Perrino, R. McGrath (2011), *Atmos. Environ.,* 48, 129 – 142, doi:10.1016/j.atmosenv.2011.07.004.

Paper 6 : Contributing author: minor role

The Eyjafjallajökull ash plume Part 2: Simulating ash cloud dispersion with REMOTE

O'Dowd C.D., S. Varghese, D. Martin, R. Flanagan, D. Ceburnis, J. Ovadnevaite, G. Martucci, J. Bialek, C. Monahan, H. Berresheim, **A. Vaishya**, T. Grigas, Z. McGraw, S.G. Jennings, B. Langmann, T. Semmler, R. McGrath (2011), *Atmos. Environ.,* 48, 143 – 151, doi:10.1016/j.atmosenv.2011.10.037.

These two papers resulted from synergetic measurements, using aerosol physical, optical, and chemical characterization instruments, of the Eyjafjallajökull ash plume and its modeled simulation using the regional climate model (REMOTE). Physicochemical properties of the ash cloud were studied for three major plume events: 20th April, 04th - 05th May, and 17th May, 2010. Ash size distribution was bimodal in nature, with a sub-µm mode diameter varying from 380-390 nm during the low-explosive phase to 180 nm during the high-explosive phase and a super-µm mode diameter at round 2.5 µm. Aerosol light absorption coefficient (σ_{abs}) increased by a factor of ~ 2 and σ_{scat} increased by an order of magnitude, as compared to background levels. In one plume event on the 17th May, σ_{scat} at 550 nm increased up to 100 Mm^{-1} which is higher than the σ_{scat} value encountered at Mace Head for most of continental outflows. σ_{scat}

increased due to increase in the accumulation mode modal diameter to 380-390 nm as compared to background levels (120-150 nm). ***The author was responsible for all of the light scattering and the light absorption measurements and for their analysis (minor role).***

3. Research Papers

3.1. Seasonal Variation of the Aerosol Light Scattering Coefficient in Marine Air of the Northeast Atlantic

Vaishya A., S.G. Jennings, C. O'Dowd (2011), Seasonal variation of the aerosol light scattering coefficient in marine air of the Northeast Atlantic, *Adv. Meteorol.*, *vol. 2011*, Article ID 170490, doi:10.1155/2011/170490.

http://www.hindawi.com/journals/amet/2011/170490/

3.2. Wind-driven influences on aerosol light scattering in north-east Atlantic air

Vaishya A., S.G. Jennings, C. O'Dowd (2012), Wind-driven influences on aerosol light scattering in North-East Atlantic air, *Geophy. Res. Lett.*, 39, L05805, doi:10.1029/2011GL050556.

http://www.agu.org/pubs/crossref/2012/2011GL050556.shtml

3.3. Light scattering enhancement factors in the marine boundary layer (Mace Head, Ireland)

Fierz-Schmidhauser R., P. Zieger, **A. Vaishya**, C. Monahan, J. Bialek, C.D. O'Dowd, S.G. Jennings, U. Baltensperger, E. Weingartner (2010), Light scattering enhancement factors in the marine boundary layer (Mace Head, Ireland), *J. Geophys. Res.*, 115 (20), D20204, doi:10.1029/2009JD013755.

http://www.agu.org/pubs/crossref/2010/2009JD013755.shtml

3.4. Warming or Cooling? The flippant effect of Organics on Sea-Spray Light-Scattering

Submitted to Nature Geoscience

Warming or Cooling? The Flippant effect of Organics on Sea-Spray Light-Scattering

Aditya Vaishya[1], Jurgita Ovadnevaite[1], Jakub Bialek[1], S. Gerard Jennings[1], Darius Ceburnis[1] & Colin O'Dowd[1]*

Primary-produced sea-spray aerosol, typically comprising sea-salt, but also enriched with organic matter in biologically-active oceanic regions, impacts the global radiative-budget through contributions to aerosol optical depth (*AOD*), at times rivaling *AOD* associated with anthropogenic aerosol pollution plumes. Here we show that sea-spray light-scattering enhancement, *f(RH)*, as a function of relative humidity *(RH)*, which typically increases with altitude, is suppressed when enriched with organic matter and a new hygroscopic (water uptake) growth-factor (*HGF*) parameterization for sea-spray is presented, revealing a dual-hygroscopicity state, flipping from high-hygroscopicity and high-*f(RH)* to low-hygroscopicity and low-*f(RH)* as the organic matter mixing volume percentage exceeds ~ 50%. In terms of organic enrichment, the effect on Top of Atmosphere (*TOA*) direct radiative forcing (*ΔF*) is to reduce the cooling contribution of sea-spray by ~ 4.5 times compared to pure sea-salt spray. For example, at wind speeds of 25 ms^{-1}, the radiative impact of pure inorganic sea salt reduces from -9 Wm^{-2} to -2 Wm^{-2}. These results highlight a significant coupling between the marine biosphere and the direct radiative budget through alteration of sea-spray chemical composition, potentially leading to accelerated global warming should biological activity increases with future projected temperature increase.

RH influences the size and chemical composition of atmospheric aerosol particles, resulting in influences on aerosol light scattering properties[1,2] and aerosol contributions to climate forcing[3,4]. Similarly so, the size and chemical composition of aerosols influences aerosol water uptake (hygroscopicity) and, ultimately, aerosol scattering properties. The influence of *RH* on aerosol particle size is quantified in physical terms by the *HGF*, defined typically as being the ratio of particle diameters under *RH* equilibrium of 90% and 20% ($D_{(RH=90\%)}/D_{(RH=20\%)}$), and in optical terms, by the scattering enhancement factor : $f(RH) = \sigma_{sc(RH=85\%)}/\sigma_{sc(RH=40\%)}$, where D is the particle diameter and σ_{sc} is the aerosol light scattering coefficient at a given wavelength.

In the clean marine environment, sea-salt is the main constituent of atmospheric aerosols[5] but organics may also dominate aerosol chemical spectra if the marine air masses advect over biologically rich waters[6,7]. Organics alter the water affinity of aerosol inorganic particles at sub-saturated *RH* and can suppress the *HGF*. It has been demonstrated recently[8] that *AOD* in clean marine air exhibits a strong power-law dependency on wind speed, pointing to a primary marine sea-spray dominating influence on *AOD*. *AOD* can reach 0.4 at λ=500 nm for moderately-high wind speeds of 18 m s^{-1} – an *AOD* comparable to, and even higher than, *AOD* levels associated with most anthropogenic pollution plumes[9]. In addition, a recent study[10] reported that the enrichment of organic matter in marine aerosol can reduce the dry-size scattering coefficient, σ_{sc}(550nm), a factor of ~ 2 due to refractive index and dry-particle size-distribution effects. Given that the marine boundary layer *RH* varies from typically *RH*~50% to *RH*~99% under cloud-free conditions, the *HGF* response to *RH* is critically important to the determination of marine aerosol haze layer optical properties. Here we report the impact of primary-organics on *HGF* and *f(RH)* in the clean marine environment using field data and present a parameterization for *HGF* as a function of *RH* and organic enrichment for use in large scale climate model studies.

Measurements were undertaken in clean North East Atlantic marine air at the Mace Head Atmospheric Research Station[11] (http://www.macehead.org), located in County Galway, Ireland (53° 19' 36'' N, 9° 54' 14'' W), offering clean-sector sampling for the wind sector 190°-300°. Meteorological records show that, on average, over 50% of the air masses arriving at the station are from the clean sector[12]. Air was sampled at 10m height from a main air inlet positioned at 80–120 m from the coastline depending on tide height. Clean marine air was selected using stringent criteria of black carbon mass concentrations less than 20 ng m^{-3} and total particle number concentration less than 700 cm^{-3} for particle sizes with D > 10 nm. Isotope analysis has demonstrated that 80% of organic carbon aerosol mass in clean air masses arriving at Mace Head is marine biogenic in origin[13].

HGF properties of aerosol were measured using a Hygroscopic Tandem Differential Mobility Analyser (*H-TDMA*)[14,15]. A higher *HGF* indicates more hygroscopic particles resulting from a higher affinity for water. The Mace Head *H-TDMA* covered dry-size *RH* = 20% to humidified *RH*= 90%. *HGF*s are determined for

School of Physics & Centre for Climate and Air Pollution Studies, National University of Ireland Galway, University Road, Galway, Ireland. * Corresponding author

dry size particles of 35, 50, 75, 110 and 165 nm. An inversion algorithm was used to retrieve the *HGF* Probability Density Function (*PDF*), corrected for multiple charges and other required associated corrections[16].

A TSI 3551 Nephelometer[17] was used to measure the σ_{sc} at 550nm wavelength. Aerosol light scattering enhancement measurements were facilitated using an in-house developed Humidograph (*RH* scanning Nephelometer) instrument. The system consists of a Nafion dryer unit which dries the sample flow to a reference low *RH* (< 40 %) and is followed by a *PM 1.0* inlet head. Ambient aerosols are mostly found in metastable state[18] and hence it is necessary to bring them to a reference dry state so as not to misinterpret their optical properties if they are on the descending branch of the hysteresis curve. A Gore-Tex humidifier then humidifies the sample flow to a desired *RH* (50 % - 90 %). The functioning of the drying unit, the humidifying unit and other sensors is identical to previously-reported systems[19].

Aerosol chemical composition was measured with the Aerodyne Research Inc. high resolution time-of-flight aerosol mass spectrometer (AMS) which provides real-time size resolved composition analysis of volatile and semi-volatile particulate matter. The combination of size and chemical analysis of sub-µm aerosol mass loading with fast time resolution makes the AMS unique and the theory of operation is well established and reported[20]. In summary, the AMS quantifies non-refractory aerosol chemical composition, covering major inorganic species such as ammonium, sulphate, nitrate, plus organic species. In addition, recent work has demonstrated that both sea-salt mass and primary marine organic mass can be retrieved from the high resolution AMS[21,22].

Table 1: Details of clean marine air masses under investigation in 2011

Type	*DoY Start*	*DoY End*	$\sigma_{sc\text{-}dry\text{-}PM1}$ *(Mm^{-1})*	R_{sp}	*BC (ng m^{-3})*	*WS (ms^{-1})*	*α*
I	68.00	68.50	8.1	0.27	9	13.7	-0.13
II	179.40	180.16	3.8	0.48	10	5.6	0.65
	181.44	182.40					
III	233.00	233.26	9.6	0.34	13	7.8	0.19
	265.33	265.62					

R_{sp} is $\sigma_{sc}(PM1)/\sigma_{sc}(PM10)$; BC is black carbon mass concentration; WS is wind speed; α is Ångström exponent (450–700 nm).

Three typical marine air mass types (see Table 1 for times and associated aerosol properties), regularly encountered over the North East Atlantic, were characterized for chemical composition, *HGF*, and *f(RH)*. Type I was characteristic of a winter marine aerosol, occurring during periods of low biological activity (LBA), in which chemical composition was composed of 68% sea-salt, 15% non-sea-salt (nss) sulphate, and 14% organics (see Figure 1). Type II was characteristics of a high biological activity (HBA) period, dominated by sulphate (56%), and with a 31% organic contribution and a 4% sea-salt contribution. The final type, Type III, is dominated by primary organic matter, during the HBA period, with a 57% contribution to mass, a 23% sulphate contribution, and a 13% sea-salt contribution. The minor aerosol species contributing to the complete non-refractory mass budget are ammonium, nitrate and methane sulphonic acid (MSA), the latter being regarded also as organic mass but given that it has a relatively high solubility, we do not include it in the general water soluble organic mass (WSOM) or water insoluble organic mass (WIOM) categories.

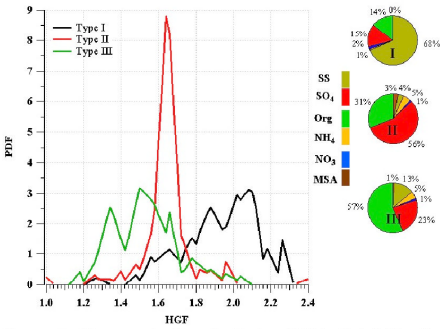

Figure 1. Hygroscopic Growth Factor (HGF) Probability Density Function (PDF) for three typical NE Atlantic clean marine air masses and associated non-refractory mass fractions.

PDF for the *HGF* distribution for the three case types is shown in Figure 1. Type I, dominated by sea-salt, has a broad *HGF* mode centered around 2.1 which is characteristic of a sea-salt dominated aerosol, albeit with a broader mode width than what would be typical of an almost pure sea-salt aerosol. Type II has a more pronounced and narrow *HGF-PDF* peak centered at approximately 1.65 while Type III exhibits *HGF-PDF* peaks at 1.35 and 1.5, typical of a low solubility organic aerosol predominance to different degrees.

In terms of *f(RH)*, as *RH* increased from 40% to 85% (*RH* of 90% was achieved for Types II & III but not for Type I - hence *f(RH)* was only analyzed up to 85%), the maximum *f(RH)* of approximately 2.8 was achieved for the sea-salt dominated Type I aerosol (Figure 2) which is higher than the value (2.22) reported for the marine boundary layer[23]. The deliquescence point for sea-salt is seen at *RH* ~ 75% while that associated with the sulphate component is seen at *RH* ~ 80%. Progressing to the predominant sulphate case with organics contributing the second highest mass contribution (Type II), we see the *f(RH)* is reduced to 1.85 at *RH*=85%. Elevated *f(RH)* values at low *RH* for this case is due to presence of organics (31 % by mass) which is responsible for water uptake by sulphate[24]. Finally, the predominant organic case, Type III, exhibits the least *f(RH)* of 1.6 at *RH*=85%. Further, an increase is not seen in *f(RH)* until *RH* exceeds 75%, at which *f(RH)* is still almost non-existent at ~ 1.05 in Type III cases compared to 1.45 for Type II, and 2.2 for Type I. Analysis of the AMS O:C ratio reveals that the organic species in Type II is much more oxidized that in Type III, distinguishing the organics in Type II as predominantly secondary and those in Type III as predominantly primary (i.e. associated with sea-spray[21]). In other words, Type I represents a dominant primary sea-salt aerosol and Type III represents a predominant

primary organic sea-spray aerosol. The effect of the enrichment of primary organics, typically with low solubility[21], is to reduce the *f(RH)* of sea-spray from 2.2 to 1.05 at *RH*=75%, and from 2.8 to 1.6 at *RH*=85%.

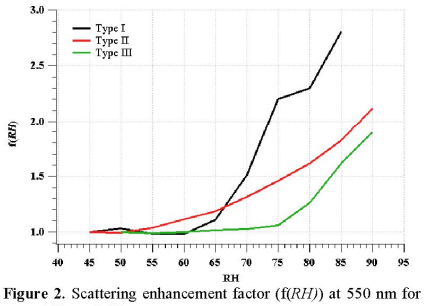

Figure 2. Scattering enhancement factor (f(*RH*)) at 550 nm for marine aerosol Types I-III.

The experimental data point towards a significant reduction in *HGF* and *f(RH)* as a function of *RH* for increasing organic mass fraction. Given that sea-spray aerosol contributes significantly to marine AOD[8], and that organic enrichment significantly influences hygroscopicity, and, ultimately, aerosol scattering, the development of a *HGF* parameterization as a function of both WIOM enrichment and *RH* is essential to elucidate the direct effect of marine aerosols.

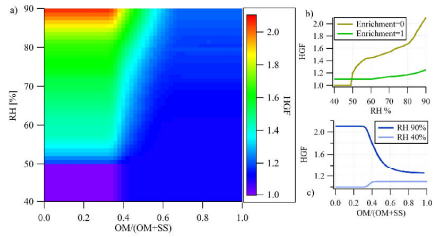

Figure 3. (a) Hygroscopic Growth Factor (*HGF*) dependence on the marine organic enrichment at different *RH*; (b) the *RH* at lower and upper limits of the enrichment - 0 and 1 respectively. Presented data is for the descending *RH* branch in the *HGF versus RH* hysteresis, thus 50% is an efflorescence point for the enrichment = 0; (c) the enrichment at lower and upper limits of *RH* - 40% and 90% respectively.

The parameterization developed herein is based on a combination of ambient measurements at Mace Head and laboratory studies of pure sea-salt aerosol particles and those enriched in primary organics. The resulting parameterization results are graphically-rendered in Figure 3. The *HGF* data was sourced from the *H-TDMA* configured both in fixed *RH* mode (with limits of 40% and 90%) for 5 sizes, and during sea-spray plumes, in scanning *RH* mode, from *RH* of 40% to 90% but for one size (165 nm). Figure 3a consolidates the combined *HGF* characterization of both laboratory studies into pure laboratory-generated compounds and field-sampled aerosol studies into a best-estimated generic marine aerosol *HGF* distribution. The dependence of *HGF* of sea-spray aerosol on the enrichment by primary marine organics over the *RH* range is presented in Figure 3a where *HGF* is seen to vary from 2.2 (at 90% *RH* and 0% enrichment) down to 1 (at *RH* 40% and 0% enrichment). The *HGF* variability at the outer lower and higher limits of enrichment, and *RH*-regimes, are presented in Figure 3b and 3c, respectively. When the enrichment is 0%, the particles behave as a pure sea-salt aerosol which experiences efflorescence at ~ 50% *RH*, indicating a change in particle phase (from liquid to solid).

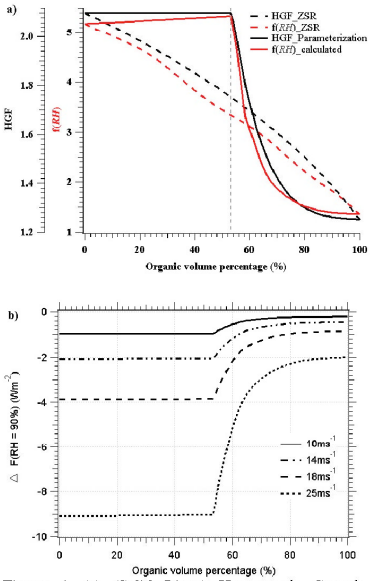

Figure 4. (a) **(Solid Lines)** Hygroscopic Growth Factor (*HGF*) dependence on the marine organic enrichment at *RH* = 90% and associated scattering enhancement for a 500 nm sea-spray particle as a function of real-world atmospheric enrichment of primary organics in sea-spray aerosol. **(Dash Lines)** Hygroscopic growth factor (*HGF*), calculated using the ZSR approach, dependence on the marine organic enrichment at *RH*=90% and associated scattering enhancement for a 500 nm sea-spray particle as a function of WIOM enrichment in sea-spray aerosol. (b) Top of Atmosphere (TOA) aerosol forcing (*ΔF*) at 90% RH as a function of Organic Volume Percentage (OVP) for four different (10, 14, 18 and 25 ms^{-1}) wind speed dependent 0.1 – 0.5 μm size distributions.

In contrast, particles enriched in organics (enrichment ~100%) do not exhibit the efflorescence point and growth factor decreases from 1.35-1.5 at 90% *RH* to 1.1 at 40%. Since particles enriched in organics do not experience the phase change, the *HGF* does not drop to the same low values as the pure sea-salt particles do. Likewise, Figure 3c represents the *HGF* dependence on sea-spray enrichment at lower and higher *RH* limits. This parameterization (summarized in Supplementary Material), reveals a unique *HGF* behavior as a function of increasing organic mass fraction at 90% *RH* – specifically, the *HGF* remains characteristic of pure sea-salt up to a specific organic enrichment threshold, specifically, ~35% in mass fraction and ~50% in volume, over and above which results in a rapid flip to a barely-*HGF* value of ~1.25.

At the other extreme of high organic enrichment, *HGF* slightly increases from 1 to 1.1 when *RH* is ~40%

as enrichment increases from 0 to 100%. This behavior is due to the phenomenon mentioned earlier – namely, organic particles do not possess an efflorescence point, and consequently, their *HGF* remains larger than 1, even at very low *RH*. *f(RH=90%)* was calculated (details in Supplementary Material), for a 500 nm particle, as a function of organic enrichment with *HGF*, density and refractive index as inputs. *HGF* was in the form of the developed primary inorganic-organic sea-spray hygroscopicity function. As shown in Figure 4a, *f(RH)* increased with increasing organic volume percentage (*OVP*) up to a threshold (53%) and thereafter decreased and approached 1.4, for *OVP* ~ 100%, which is comparable to Type III *f(RH)*. Model calculations of *HGF* (using the *Zdanovskii, Stokes and Robinson (ZSR)* approach[25]) and *f(RH)*, using real inputs of *HGF* for extreme *OVPs* (ie. 0% and 100%), for intermediate *OVPs* were not compatible with field results.

RH dependent *TOA* - ΔF calculations (details in Supplementary Material) were performed for size distributions (0.1 -0.5 µm) at four different wind speeds (10, 14, 18 and 25 ms^{-1}) and at *RH* = 90% as shown in Figure 4b. For organic enrichment greater than 53% a notable reduction occurs in the negative radiative forcing, reaching a maximum decrease by ~ 4.5 times for enrichments of 80% organics.

We have reported, for the first time, the effect of organic matter enrichment in sea-spray aerosol and have demonstrated an unusual effect of enrichment on both aerosol hygroscopicity and RH-driven *f(RH)* whereby, once organic volumetric percentage exceeds 53%, the *f(RH)* and *HGF* values flip from a maximum hydrated value to minimum hydrated, or more or less, dry values. Such changes in *f(RH)* are reflected in *TOA* - ΔF for organics enriched sea-spray, were ΔF is enhanced by a factor of ~ 4.5 as compared to pure sea-salt spray. This important new finding strongly pointing towards an important link between oceanic biological activity, primary organic matter enrichment in sea-spray aerosol, and suppression of marine aerosol *AOD*, leading to increase global warming rates should marine productivity increases with project global temperature increase.

Contribution of authors: AV developed the scattering humidograph instrument and collected, processed and analysed all related data, performed radiative forcing calculations and contributed to writing part of the manuscript. JO provided the AMS data and developed the *HGF* parameterization as a function of organic enrichment. JB provided the *HGF* data to underpin the parameterization development. SGJ co-supervised AV's scattering work with COD and. contributed in model calculations of *f(RH)*. DC contributed to organizing and overseeing the field and laboratory measurement programme and to the development of the *HGF* parameterization. COD wrote the manuscript, proposed the idea for coupling *HGF* and scattering results and, generally, oversaw all aspects of the work programme and scientific development and integration.

Acknowledgements. The work described in this paper was supported by the EC FP6 Projects EUSAAR (FP6-026140) and GEOmon (FP6-2005-Global-4-036677) and the ESA-OSSA ESRIN Project Contract No. 4000104514/11/I-AM. HEA PRTLI4 and EPA STRIVE funding is also acknowledged. Harald Berresheim (NUIG) is acknowledged for providing part of the AMS data used in parameterization. Ciaran Monahan (NUIG) is acknowledged for providing the size distribution data.

1. Covert, D. S., Charlson, R. J. & Ahlquist, N. C. A Study of the Relationship of Chemical Composition and Humidity to Light Scattering by Aerosols. *J. Appl. Met.* **11**, 968-976, doi:10.1175/1520-0450(1972)011<0968%3AASOTRO>2.0.CO%3B2 (1972).
2. Tang, I. N. Chemical and size effects of hygroscopic aerosols on light scattering coefficients. *J. Geophys. Res.* **101**, 19245-19250, doi:10.1029/96JD03003 (1996).
3. Markowicz, K. M. *et al.* Influence of relative humidity on aerosol radiative forcing: An ACE-Asia experiment perspective. *J. Geophys. Res.* **108**, D23, doi:10.1029/2002GL015767 (2003).
4. Schwartz, S. E. The Whitehouse effect - Shortwave radiative forcing of climate by anthropogenic aerosols: An overview. *J. Aerosol Sci.* **27**, 359-382 (1996).
5. O'Dowd, C. D. & Smith, M. H. Physicochemical properties of aerosols over the northeast Atlantic: evidence for wind-speed-related submicron sea-salt aerosol production. *J. Geophys. Res.* **98**, 1137-1149, doi:10.1029/92JD02302 (1993).
6. O'Dowd, C. D. *et al.* Biogenically driven organic contribution to marine aerosol. *Nature* **431**, 676-680, doi:10.1038/nature02959 (2004).
7. Ovadnevaite, J. *et al.* Detecting high contributions of primary organic matter to marine aerosol: A case study. *Geophys. Res. Lett.* **38**, L02807, doi:10.1029/2010GL046083 (2011).
8. Mulcahy, J. P., O'Dowd, C. D., Jennings, S. G. & Ceburnis, D. Significant enhancement of aerosol optical depth in marine air under high wind conditions. *Geophys. Res. Lett.* **35**, L16810, doi:10.1029/2008GL034303 (2008).
9. Dubovik, O. *et al.* Variability of absorption and optical properties of key aerosol types observed in worldwide locations. *J. Atmos. Sci.* **59**, 590-608 (2002).
10. Vaishya, A., Jennings, S. G. & O'Dowd, C. Wind-driven influences on aerosol light scattering in north-east Atlantic air. *Geophys. Res. Lett.* **39**, L05805, doi:10.1029/2011gl050556 (2012).
11. O'Connor, T. C., Jennings, S. G. & O'Dowd, C. D. Highlights of fifty years of atmospheric aerosol research at Mace Head. *Atmos. Res.* **90**, 338-355, doi:10.1016/j.atmosres.2008.08.014 (2008).
12. Jennings, S. G. *et al.* Mace Head Atmospheric Research Station - Characterization of aerosol radiative parameters. *Boreal Environ. Res.* **8**, 303-314 (2003).
13. Ceburnis, D. *et al.* Quantification of the carbonaceous matter origin in submicron marine aerosol by 13C and 14C isotope analysis. *Atmos. Chem. Phys.* **11**, 8593-8606, doi:10.5194/acp-11-8593-2011 (2011).
14. Nilsson, E. *et al.* Development of an H-TDMA for long-term unattended measurement of the hygroscopic properties of atmospheric aerosol particles. *Atmos. Meas. Tech.* **2**, 313-318 (2009).
15. Rader, D. J. & McMurry, P. H. Application of the tandem differential mobility analyzer to studies of droplet growth or evaporation. *J. Aerosol Sci.* **17**, 771-787 (1986).
16. Gysel, M., McFiggans, G. B. & Coe, H. Inversion of tandem differential mobility analyser (TDMA) measurements. *J. Aerosol Sci.* **40**, 134-151, doi:10.1016/j.jaerosci.2008.07.013 (2009).
17. Ahlquist, N. C. & Charlson, R. J. A new instrument for evaluating the visual quality of air. *J. Air Poll. Control Assoc.* **17**, 467-469 (1967).
18. Rood, M. J., Shaw, M. A., Larson, T. V. & Covert, D. S. Ubiquitous nature of ambient metastable aerosol. *Nature* **337**, 537-539 (1989).
19. Fierz-Schmidhauser, R. *et al.* Measurement of relative humidity dependent light scattering of aerosols. *Atmos. Meas. Tech.* **3**, 39-50, doi:10.1029/2003JD003405 (2010).
20. Jimenez, J. L. *et al.* Ambient aerosol sampling using the Aerodyne aerosol mass spectrometer. *J. Geophys. Res.* **108**, D7, doi:10.1029/2001JD001210 (2003).
21. Ovadnevaite, J. *et al.* Primary marine organic aerosol: A dichotomy of low hygroscopicity and high CCN activity. *Geophys. Res. Lett.* **38**, L21806, doi:10.1029/2011gl048869 (2011).
22. Ovadnevaite, J. *et al.* New findings on the effect of wind speed on submicron sea salt mass concentrations and source fluxes *J. Geophys. Res.*, Accepted manuscript (2012).
23. Fierz-Schmidhauser, R. *et al.* Light scattering enhancement factors in the marine boundary layer (Mace Head, Ireland). *J. Geophys. Res.* **115**, D20204, doi:10.1029/2009JD013755 (2010).
24. Pósfai, M., Xu, H., Anderson, J. R. & Buseck, P. R. Wet and dry sizes of atmospheric aerosol particles: An AFM-TEM study. *Geophys. Res. Lett.* **25**, 1907-1910 (1998).
25. Stokes, R. H. & Robinson, R. A. Interactions in aqueous nonelectrolyte solutions. I. Solute-solvent equilibria. *J. Phys. Chem.* **70**, 2126-2131 (1966).

Supplementary Material

S1. Hygroscopic growth factor (*HGF*) parameterization as a function of both organic enrichment and relative humidity (*RH*):

Sea-salt *HGF* as a function of *RH*:

The sea-salt *HGF* dependence on *RH* used in this parameterization (Figure S1) was obtained using artificial SIGMA sea-salt dissolved in deionized water. The solution was nebulized with a TSI atomizer (model 3076) and then directed to the H-TDMA. In order to characterise the *HGF* behaviour with decreasing *RH* (i.e. to find particle efflorescence rather than particle deliquescence), an additional humidifier and a dryer system was introduced between the first and second DMA in the H-TDMA. As a result, after the size selection with the first DMA, aerosol particles were humidified above the deliquescence point and then dried to the required *RH* using a Nafion drier (Perma Pure PD-200T). By this procedure, we were able to reproduce the sea-salt efflorescence point. The reducing *RH* branch is more appropriate for marine ambient conditions (it is very unlikely that sea-spray aerosol could reach the efflorescence point in the marine environment, thus first humidifying particles above deliquescence and only then, drying would mimic the ambient conditions). Figure S1 represents the limiting condition for zero organic mass enrichment.

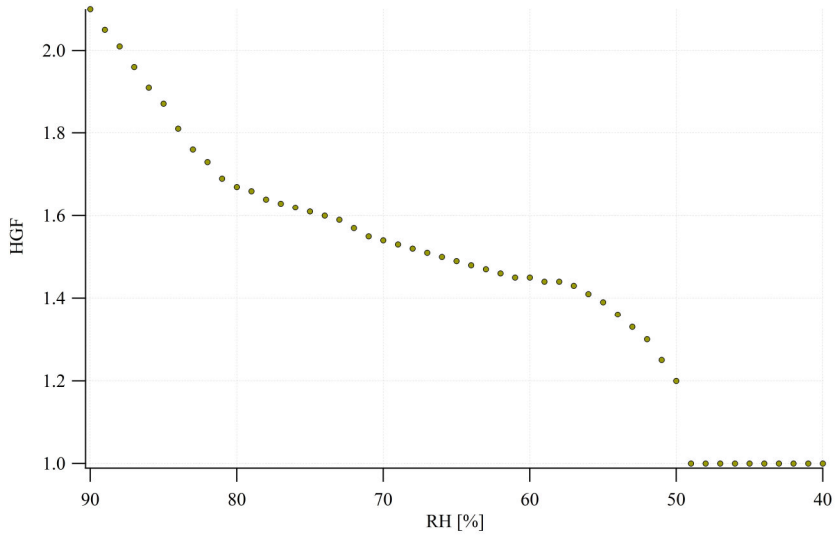

Figure S1. Sea-salt hygroscopic growth factor (*HGF*) dependence on *RH* for the reduction branch in *RH* hysteresis.

S2. *HGF* dependence on different enrichments at 90% *RH*:

The *HGF* dependence on different enrichments at 90% *RH* was obtained from the long term concurrent AMS and HTDMA measurements at Mace Head (Figure S2). Figure S2 reveals a unique *HGF* behavior as a function of increasing organic mass fraction at 90% *RH* – specifically, the *HGF* remains characteristic of pure sea-salt up to a specific organic enrichment threshold, specifically, ~0.35 in mass fraction and ~0.5 in volume, over and above which results in a rapid flip to a barely-*HGF* of ~1.25. This dependency could be expressed with the following relationship:

$$HGF(x) = \begin{cases} 2.1, & \text{if } x < 0.35 \\ 1.25 + 23.9 * \exp(-9.4 * x), & \text{if } x \geq 0.35 \end{cases}$$

Eq. **S1**

where x represents the enrichment.

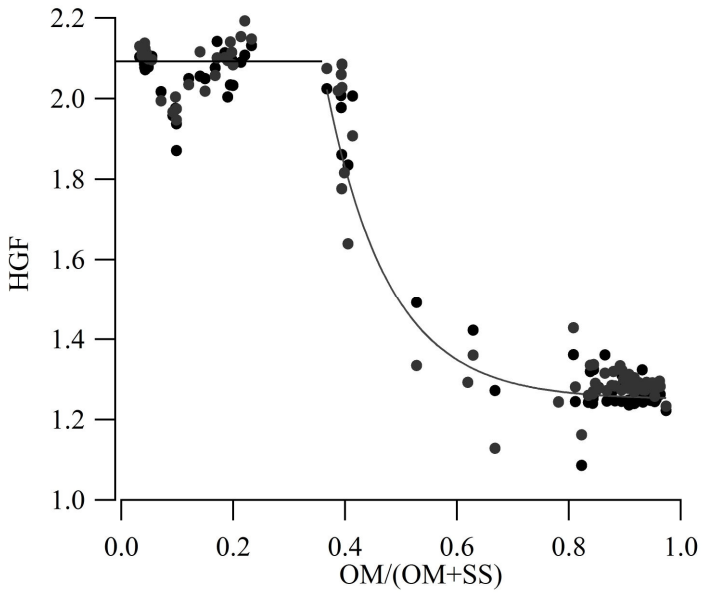

Figure S2. *HGF* parameterization vs. aerosol enrichment in organics at 90% *RH*.

S3. *HGF* variability with different enrichments at different *RH*:

The intermediate values for the different levels of enrichment at different *RH* were found by running HTDMA in the scanning *RH* mode for the ambient aerosol measurements. Some examples are presented in Figure S3 and S4. Considering, that ambient aerosol is usually a mixture of sea-spray and secondary sulphate, the *HGF* filtering for *HGF* modes typical for sulphate particles at a particular *RH* was applied. This procedure could have led to filtering out the sea spray particles, which had *HGF* equivalent to the sulphate *HGF* (internal mixture of sea-salt and organics). However, it was necessary in order to acquire sea-spray *HGF* from the external ambient aerosol mixture.

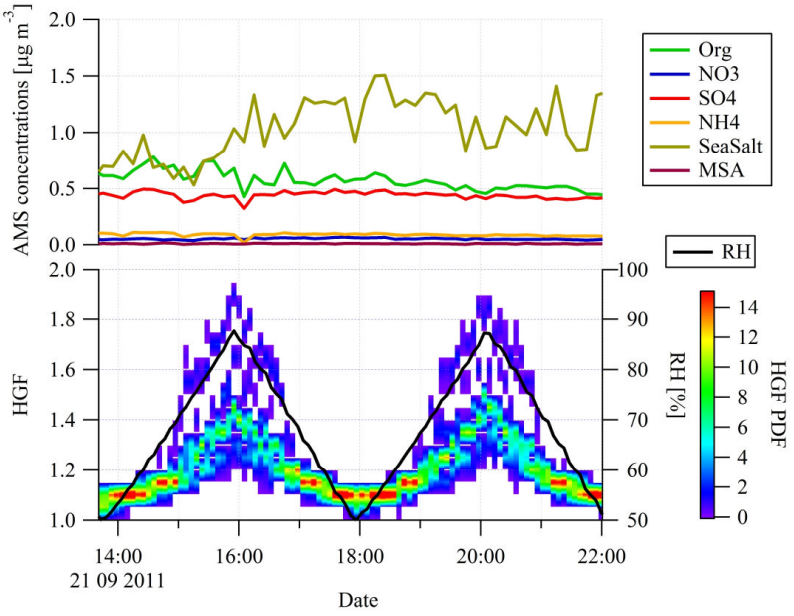

Figure S3. Low enrichment in organics.

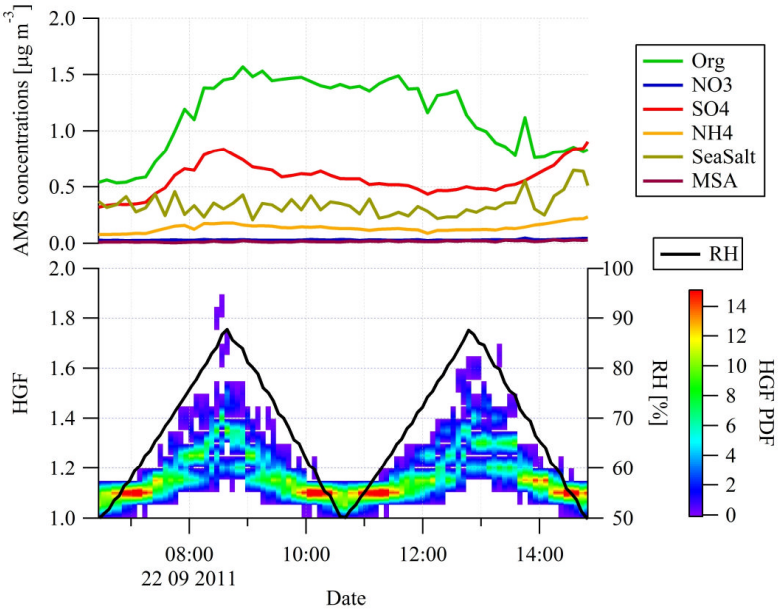

Figure S4. High enrichment in organics.

S4. Overall *HGF* parameterization:

Combined data of both laboratory and ambient experiments are presented in Table S1. Table S1 represents Figure 3a in the manuscript.

Table **S1**. *HGF* dependency on the organic enrichment over a range of *RH*.

RH (%)	40.00	45.00	50.00	55.00	60.00	65.00	70.00	75.00	80.00	85.00	90.00
Org/(Org+SS)											
0.00	1.00	1.00	1.20	1.39	1.45	1.49	1.54	1.61	1.67	1.87	2.10
0.05	1.00	1.00	1.20	1.39	1.45	1.49	1.54	1.61	1.67	1.87	2.10
0.10	1.00	1.00	1.20	1.39	1.45	1.49	1.54	1.61	1.67	1.87	2.10
0.15	1.00	1.00	1.20	1.39	1.45	1.49	1.54	1.61	1.67	1.87	2.10
0.20	1.00	1.00	1.20	1.39	1.45	1.49	1.54	1.61	1.67	1.87	2.10
0.25	1.00	1.00	1.20	1.39	1.45	1.49	1.54	1.61	1.67	1.87	2.10
0.30	1.00	1.00	1.20	1.39	1.45	1.49	1.54	1.61	1.67	1.87	2.10
0.35	1.00	1.00	1.20	1.39	1.45	1.49	1.54	1.61	1.67	1.87	2.10
0.41	1.10	1.10	1.10	1.21	1.26	1.31	1.35	1.41	1.50	1.63	1.77
0.45	1.10	1.10	1.10	1.17	1.21	1.25	1.29	1.34	1.42	1.53	1.60
0.51	1.10	1.10	1.10	1.12	1.15	1.18	1.21	1.25	1.32	1.40	1.45
0.55	1.10	1.10	1.10	1.10	1.12	1.15	1.17	1.21	1.26	1.32	1.38
0.61	1.10	1.10	1.10	1.10	1.10	1.13	1.15	1.17	1.20	1.24	1.33
0.65	1.10	1.10	1.10	1.10	1.10	1.12	1.14	1.16	1.18	1.21	1.30
0.71	1.10	1.10	1.10	1.10	1.10	1.12	1.14	1.16	1.18	1.20	1.28
0.80	1.10	1.10	1.10	1.10	1.10	1.12	1.14	1.16	1.17	1.20	1.26
0.86	1.10	1.10	1.10	1.10	1.10	1.12	1.14	1.16	1.17	1.20	1.26
0.90	1.10	1.10	1.10	1.10	1.10	1.12	1.14	1.16	1.17	1.20	1.26

0.96	1.10	1.10	1.10	1.10	1.10	1.12	1.14	1.15	1.17	1.20	1.25
1.00	1.10	1.10	1.10	1.10	1.10	1.12	1.14	1.15	1.17	1.20	1.25

S5. Mie modeling and radiative forcing calculations:

Aerosol light scattering coefficient (σ_{sc}) and backscattering coefficient (σ_{bsc}) calculations were performed using standard Mie code[1,2]. Refractive index of sea-salt[3] = 1.5-i10^{-8} and for WIOM = 1.48[4] was used as well as density in g cm^{-3} of sea-salt[5] = 2.1 and WIOM[6] = 1.0. For the multi-component aerosol, the refractive index was calculated using volume weighting of dry refractive indices.

RH dependent Top of Atmosphere (*TOA*) direct radiative forcing (ΔF) calculations were performed using the formulation by Haywood and Shine[7] as described by Equation S2.

$$\Delta F(RH) = -DS_0 T_{at}^2 (1 - A_c)\omega_0(RH)\beta(RH)\delta(RH)\left[(1 - R_s)^2 - \left(2R_s / \beta(RH)\right)\left(\frac{1}{\omega_0(RH)} - 1\right)\right]$$

Eq. S2

where D is the fraction day length (0.5), S_0 is the solar constant (1370 W m^{-2}), T_{at} is the atmospheric transmission (0.76), A_c is the fractional cloud cover (0.6), ω_0 is *RH* dependent single scattering albedo, β is *RH* dependent up-scatter fraction, δ is *RH* dependent aerosol optical thickness, and R_s is the surface reflectance. β was parameterized[8] from the backscatter fraction (b). In the present case, since the underlying surface is ocean, R_s = 0.06 was used[9]. An aerosol absorption coefficient equivalent to 20 ng m^{-3} of black carbon concentration was used, which is representative of a clean marine environment[10]. ω_0, b, and σ_{sc} were calculated, for SMPS size distribution for particle diameter 0.1 – 0.5 μm at four different wind speeds (10, 14, 18 and 25 ms^{-1}), using a Mie scattering code[1,2]. δ was calculated by integrating σ_{sc} from sea level up to a marine boundary layer height of 1000 m, assuming a well mixed column of

aerosol with identical physical, chemical and optical properties. ΔF calculations were performed at 90% *RH* and as a function of *WIOM* enriched sea-salt using the developed *HGF* parameterization, presented in section S2.

1 Mätzler, C. MATLAB Functions for Mie Scattering and Absorption. Report No. 2002-11, (2002).

2 Bohren, C. F. & Huffman, D. R. *Absorption and scattering of light by small particles*. J Wiley & Sons, New York, (1983).

3 Kent, G. S., Yue, G. K., Farrukh, U. O. & Deepak, A. Modeling atmospheric aerosol backscatter at CO2 laser wavelengths. 1: Aerosol properties, modeling techniques, and associated problems. *Appl. Opt.* **22**, 1655-1665 (1983).

4 Nessler, R., Weingartner, E. & Baltensperger, U. Adaptation of dry nephelometer measurements to ambient conditions at the Jungfraujoch. *Environ. Sci. Technol.* **39**, 2219-2228 (2005).

5 Tang, I. N., Tridico, A. C. & Fung, K. H. Thermodynamic and optical properties of sea salt aerosols. *J. Geophys. Res.* **102**, 23,269-23,275 (1997).

6 Cavalli, F. *et al.* Advances in characterization of size-resolved organic matter in marine aerosol over the North Atlantic. *J. Geophys. Res.* **109**, D24215, doi:10.1029/2004jd005137 (2004).

7 Haywood, J. M. & Shine, K. P. The effect of anthropogenic sulfate and soot aerosol on the clear sky planetary radiation budget. *Geophys. Res. Lett.* **22**, 603-606 (1995).

8 Wiscombe, W. J. & Grams, G. W. The backscattered fraction in two-stream approximations. *J. Atmos. Sci.* **33**, 2440-2451 (1976).

9 Payne, R. E. Albedo of the sea surface. *J. Atmos. Sci.* **29**, 959-970 (1972).

10 O'Dowd, C. D., Smith, M. H. & Jennings, S. G. Submicron particle, radon, and soot carbon characteristics over the northeast Atlantic. *J. Geophys. Res.* **98**, 1123-1135, doi:doi:10.1029/92JD02387 (1993).

3.5. The Eyjafjallajökull ash plume Part I: Physical, chemical and optical characteristics

O'Dowd C.D., D. Ceburnis, J. Ovadnevaite, G. Martucci, J. Bialek, C. Monahan, H. Berresheim, **A. Vaishya**, T. Grigas, S.G. Jennings, P. McVeigh , S. Varghese, R. Flanagan, D. Martin, E. Moran, K. Lambkin, T. Semmler, C. Perrino, R. McGrath (2011), The Eyjafjallajökull ash plume Part I: Physical, chemical and optical characteristics, *Atmos. Environ.,* 48, 129 – 142, doi:10.1016/j.atmosenv.2011.07.004.

http://www.sciencedirect.com/science/article/pii/S1352231011007059

3.6. The Eyjafjallajökull ash plume Part 2: Simulating ash cloud dispersion with REMOTE

O'Dowd C.D., S. Varghese, D. Martin, R. Flanagan, D. Ceburnis, J. Ovadnevaite, G. Martucci, J. Bialek, C. Monahan, H. Berresheim, **A. Vaishya**, T. Grigas, Z. McGraw, S.G. Jennings, B. Langmann, T. Semmler, R. McGrath (2011), The Eyjafjallajökull ash plume Part 2: Simulating ash cloud dispersion with REMOTE, *Atmos. Environ.,* 48, 143 – 151, doi:10.1016/j.atmosenv.2011.10.037.

http://www.sciencedirect.com/science/article/pii/S1352231011011113

4. Conclusions

Aerosol light scattering properties and their dependency on relative humidity, wind speed and chemical composition were studied for aerosols associated with North-East Atlantic marine air masses. Objectives of the present study and findings / conclusions addressing the objectives are presented below.

- Is there a seasonal pattern exhibited by aerosol scattering properties in the clean marine environment of the North-East Atlantic? If yes, then what are the driving forces behind the observed patterns?

Analysis of ten years (2001-2010) of aerosol light scattering data, for clean marine air masses arriving at the Mace Head Atmospheric Research Station, revealed that the aerosol light scattering coefficient (σ_{scat}) and the Ångström exponent ($\mathring{A}$) exhibit a seasonal pattern. The observed seasonal cycle in σ_{scat}, with a maximum of 35.3 ± 20.0 Mm^{-1} in January and a minimum of 13.7 ± 8.4 Mm^{-1} in July, was mainly driven by the contribution of wind-speed generated sea-spray aerosols particles in the marine boundary layer. This is indicated by a high positive correlation coefficient of 0.88 between σ_{scat} and wind-speed. Also, a near seven fold increase in the percentage occurrence of larger $\mathring{A}$ values (>1.2) and a high positive correlation coefficient of 0.82 between percentage occurrence of larger $\mathring{A}$ values (>1.2) and percentage occurrence of smaller σ_{scat} values (5-15 Mm^{-1}) indicates an important contribution of non-sea-salt (nss) sulphate and sea-spray enriched with organics to σ_{scat} in the summer months.

- Can one quantify wind-driven influences on aerosol light scattering? Does sea-spray and ocean biota affect scattering magnitudes or their dependence on wind-speed in different seasons?

The σ_{scat} and σ_{bscat} dependency on wind-speed (U) was quantified using ten years (2001-2010) of aerosol light scattering and meteorological datasets. The σ_{scat} and σ_{bscat} was found to be dependent on ~ U^2 for both the winter (Low Biological Activity – LBA) and the summer (High Biological Activity – HBA) seasons, for clean marine North-East Atlantic air masses. A high correlation coefficient (~0.95) was found for both σ_{scat} and σ_{bscat}. A dominant super-µm size particle mode was present at all wind speeds during the LBA-period, as indicated by low Ångström exponent (α) values. LBA-period radiative values, σ_{scat} and σ_{bscat}, are twice or more than that for the HBA-period. This difference, up to 96%, can be explained by a combined effect of size distribution and refractive index. Refractive index difference between LBA-HBA periods, resulting from organic enrichment of sea-spray aerosols during the HBA-period, alone can account for 70% of the observed differences in σ_{scat}. σ_{scat} values at 25ms^{-1} was ~ 70Mm^{-1} which is considerably higher than the σ_{scat} values encountered under polluted air masses in the same region.

- How does relative humidity affect the light scattering properties of aerosols in clean and polluted marine environments?

Light scattering enhancement factors ($f(RH, \lambda)$) were determined for two major air mass types, clean marine and modified / polluted marine, arriving at the Mace Head Atmospheric Research Station. Values of f(85%, 550nm) were 2.22 and 1.77 for clean and polluted air masses, respectively. Higher values of $f(RH, \lambda)$ for the clean marine air masses are due to a relatively large contribution of primary produced sea-spray aerosols, which has higher affinity for water. For the polluted air masses, the $f(RH, \lambda)$ values are suppressed due to the presence of anthropogenic organic species which suppress the water uptake of aerosol particles. Also, clean marine air masses show a distinct hysteresis behaviour: f(55%, 550nm) values for dehydration, which are on average 35% higher than that for hydration, which is not prominent in polluted air masses. The single scattering albedo (ω_0) increased by ~ 5%, as compared to dry conditions, for polluted air masses. This is due to the addition of water which dilutes the effect of hydrophobic species and hence increases ω_0. The backscatter fraction (b)

decreased by about 20%, as compared to dry conditions, for both air masses due to an increase in the aerosol particle size parameter.

- What role does aerosol chemical composition play in the response of aerosols to changes in relative humidity? What are the radiative implications of this?

Using the in-house developed state-of-the-art Wet-Nephelometer instrument (Humidograph), we have reported, for the first time, the effect of organic matter enrichment in sea-spray aerosol on aerosols hygroscopicity and aerosol light scattering properties. The effect of enrichment of primary organics, typically with low solubility, is to reduce the *f(RH)* of sea-spray aerosol from 2.2 to 1.05 at *RH*=75%, and from 2.8 to 1.6 at *RH*=85%. We have also demonstrated an unusual effect of enrichment on both aerosol hygroscopicity and *f(RH)* whereby, once organic volumetric percentage exceeds 53%, the *f(RH)* and hygroscopic growth factor (*HGF*) values flip from a maximum hydrated value to minimum hydrated, or more or less dry value. Model studies show that the radiative impact of organic enriched sea-spray is to reduce the Top of Atmosphere (*TOA*) direct radiative forcing (ΔF) by ~ 4.5 times as compared to pure sea-salt spray. This significant finding reveals a strong coupling between marine organics and the direct radiative budget, through alteration of sea-spray chemical composition. This could potentially lead to accelerated global warming rates should biological activity increase with future projected temperature increases.

- What are the optical characteristics of ash cloud aerosols?

The Eyjafjallajökull volcanic ash plume was detected at the Mace Head Atmospheric Research Station during the months of April-May, 2010. Aerosol optical properties, light absorption coefficient (σ_{abs}) and light scattering coefficient (σ_{scat}), were elevated during the plume events. σ_{abs} increased by a factor of ~ 2, while σ_{scat} increased by an order of magnitude, as compared to background levels. The increase in σ_{scat} is due to a shift in the accumulation

mode modal diameter from 120-150 nm (background levels) to 380-390 nm. The increase in σ_{abs} is mainly due to a higher concentration of crustal elements in the ash plume. σ_{scat} values at 550 nm increased up to 100 Mm^{-1} in one of the ash cloud plumes, thus overriding the σ_{scat} values normally encountered at Mace Head for most of the continental outflows.

The results described above contribute significantly towards a better understanding and improved physicochemical characterization of aerosols pertaining to the marine environment. Analysis of ten years of aerosol light scattering data indicates a wind-driven seasonal pattern in σ_{scat} and it also suggests a role of nss sulphate and organics in suppressing aerosol light scattering. Further studies reveal that σ_{scat} and σ_{bscat} are indeed dependent upon U through a power law with dependency of $\sim U^2$ and that, LBA radiative properties are twice that of HBA radiative properties. This difference in LBA-HBA radiative properties is explained, up to 96%, by the combined effect of size distribution and refractive index (or chemical composition) whereas refractive index alone accounts for 70% of the observed differences.

Obtaining of an in-depth understanding of seasonal characteristics of scattering properties of marine aerosols and their wind-driven influences has led to a study and quantification of the effect of *RH* on aerosol scattering properties. Clean marine air masses depict hysteresis behaviour in *f(RH)* with a value of *f(55%)* for the dehydration branch, which is 35% higher on average than for the hydration branch. Mie scattering modelling with real world size distributions and HGF as input parameters leads to reasonable predictions of *f(RH)* values. *RH* suppresses the backscatter fraction (b) by ~ 20% and increases ω_0 on average by 1-5% at 85% as compared to dry conditions. Measurement of scattering properties of aerosols at varying *RH* using an in-house developed Humidograph system revealed a dual-hygroscopicity state of sea-spray aerosols. The effect of enrichment by marine organics is to suppress the *f(RH)* by a factor of about three. The dual behaviour, flipping from high hygroscopicity and high *f(RH)* to low hygroscopicity and low *f(RH)*, of organic enriched sea-spray aerosol impact the *TOA-ΔF* values. The effect of organic enrichment on *TOA-ΔF* values is to

decrease it, on a negative scale, by a factor of ~4.5 as compared to pure sea-salt spray, thus significantly reducing the cooling effect of sea-salt spray.

Further work is required to better understand intensive aerosol optical properties and their seasonal behaviour in the clean marine environment. A logical approach towards this may be to characterize the air masses in terms of the radiative properties (both intensive and extensive) and to further supplement them with chemical composition and other microphysical information. All of this information can be better utilized as inputs to aerosol radiative modelling along with a developed *HGF* parameterization of sea-spray aerosol, thus leading to radiative forcing estimates of the *TOA-ΔF*. This will help in advancing our knowledge base about radiative processes in the atmosphere involving aerosol species and their implications on future climate change.

Appendix

A.1. Introduction

Light scattering techniques are useful tools for studying the hygroscopic and deliquescent properties of aerosol. Aerosol light *scattering coefficient* (σ_{scat}^{λ}) and *backscattering coefficient* (σ_{bscat}^{λ}) can be measured continuously using any commercially available Integrating Nephelometer for e.g. TSI Inc., Model – 3551 (IN-3551) and 3563 (IN-3563), Ecotech Aurora 3000 etc. Due to its closed chamber design, high sensitivity, relatively simple calibration technique, and easily replaceable components it is suitable for long term air quality monitoring [*Anderson et al.*, 1996; *Bodhaine et al.*, 1991; *Müller et al.*, 2011]. A detailed review of design philosophy and possible applications of the Integrating Nephelometer is presented by *Heintzenberg and Charlson* [1996]. Figure A.1 shows the schematic of Nephelometer geometry which is used for calculating the aerosol scattering properties.

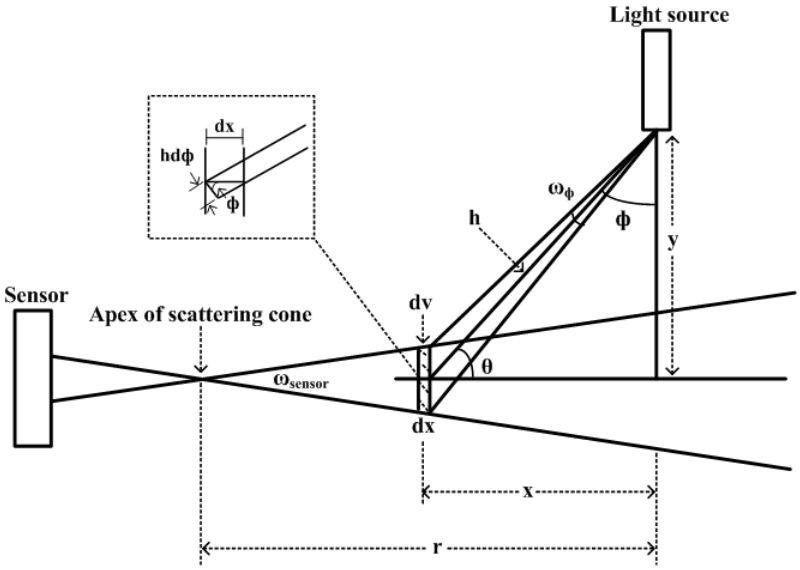

Figure A.1. Schematic of Nephelometer geometry (Redrawn from Anderson et al., 1996).

A set of closure experiments to study the performance characteristics of IN-3563 has been reported by *Anderson et al.* [1996]. For optimal performance of the IN-3563, *Anderson and Ogren* [1998] have suggested a calibration approach using air and CO_2 as preferred calibration gases and also periodically removing the coarse mode particles from the sample to enable independent study of accumulation and coarse mode contributions to light scattering.

Out of many possible applications of the Integrating Nephelometer as described by *Heintzenberg & Charlson* [1996], and *Anderson et al.* [1996], the knowledge of *f(RH)* (*scattering enhancement factor*) has particular importance in radiative transfer and climate related studies [*Quinn et al.*, 1996; *Ramaswamy et al.*, 2001; *Schwartz*, 1996].

A.2. Nephelometer non-idealities

The IN-3563 Integrating Nephelometer measures aerosol scattering properties based on following assumptions:

i. Nephelometer senses scattering from 0^0 to 180^0.
ii. Volume elements act as a point source of scattered light.
iii. Sensing volume is illuminated by a point source of isotropic light.
iv. Nephelometer responds to monochromatic radiation at exact nominal wavelength.

All of the above mentioned assumptions are for an ideal Nephelometer. In practice, though, these assumptions are not followed by the model IN-3563 and hence result in systematic uncertainties in the measurement of aerosol scattering properties. Uncertainties are estimated to be less than 10 % for accumulation mode particle sizes (volume mean diameters, d between 0.2 μm and 0.4 μm) and between 20-50 % for coarse mode particles (d >1 μm) [*Anderson et al.*, 1996]. The effect of angular truncation in sensing the total scattering signal is minimal for sub-micrometer aerosol particles (d <1 μm) [*Quirantes et al.*, 2008]. The sampling system or aerosol transport system may introduce discrepancies

between modeled and measured σ_{scat}^{λ} values [*Kleefeld et al.*, 2002], in addition to discrepancies introduced due to Nephelometer non-idealities.

Uncertainties originated from above mentioned non-idealities of the Nephelometer can be minimized by applying the correction factors obtained using the wavelength dependency of scattering [*Bond et al.*, 2009]. Corrections factors can vary depending on the size distribution and refractive index of the aerosol particles [*Quirantes et al.*, 2008].

A temperature gradient inside the Nephelometer measurement chamber (Figure A.2) due to heating by the lamp is source for another major uncertainty in the accurate measurement of aerosol scattering coefficient, because, it affects the physical and hence scattering properties of the aerosols. This source of uncertainty can be much larger than the systematic uncertainty introduced by the non-ideal light sensing geometry of the Nephelometer [*Müller et al.*, 2009].

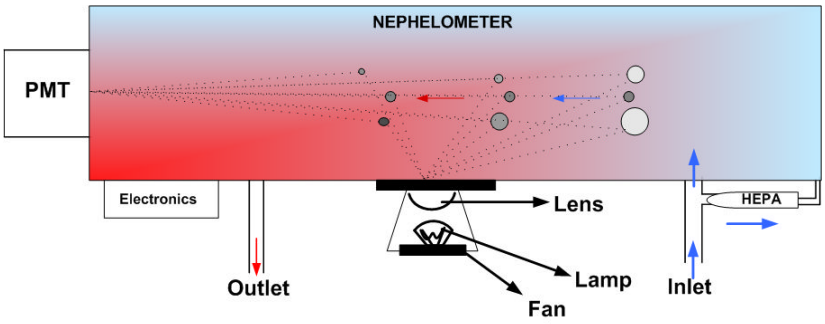

Figure A.2. Temperature gradient inside the Nephelometer measurement chamber.

During a field campaign (from 16th January, 2009 to 16th February, 2009) at the Mace Head Atmospheric Research Station, it was found that on an average a temperature difference (ΔT), measured using the temperature sensors at the inlet and in the measurement chamber, of 6.0 ^{0}C between the inlet and the measurement chamber of IN-3563 reduced the *RH* of the sample air by 10.4% *RH* units (Figure A.3). In extreme cases, ΔT was found to be 7.4 ^{0}C and ΔRH 28.97 %, with the maximum ΔT not necessarily related to maximum ΔRH. Following the design modifications suggested by *Heintzenberg and Erfurt,* [2000], a set of alterations in the existing IN-3561 is made and is detailed in the next section.

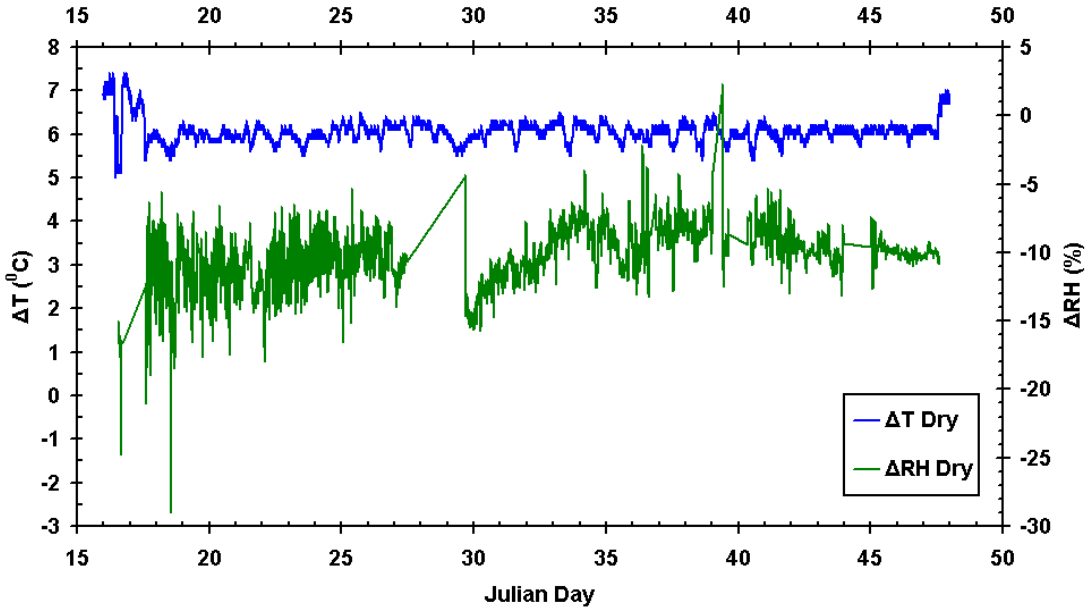

Figure A.3. *ΔT* and *ΔRH* between the inlet and measurement chamber of the Nephelometer.

A.3. Development of the Humidograph system

It is necessary to measure *f(RH)* values along with other vital aerosol optical properties and meteorological parameters in order to study the hygroscopic behaviour of aerosols for different *air-masses* and seasons. For such purpose, design of a Humidograph system has been conceived and a block diagram for the same is shown in Figure A.4. The main components of the Humidograph system are: Nafion dryer, Gore-Tex humidifier, and the HORST temperature regulator. Figure A.5 shows in detail the Humidograph components along with other accessories. Ambient air is drawn in the system through the community sampling tube (main duct) at a rate of 33.3 *LPM* (litres per minute). Ambient aerosols are mostly found in a metastable state [*Rood et al.*, 1989] and hence it is necessary to bring them to a reference dry state before measuring their optical properties. Drying is required to avoid misinterpreting the optical properties of hygroscopic aerosols if they are on the descending branch of the hysteresis curve. The principal mechanism in the drying unit is based on the characteristic of the Nafion tube used which allows water vapour to permeate through the wall of the tube if there is a difference of vapour pressure across the

wall. A Nafion dryer (Perma Pure FC-150-480-7PP) is used to dry the sample flow to a reference dry state (*RH* < 40 %) at a flow rate of 33.34 *LPM*. Rotronic Hygroclip (HC2-S) *RH* and *T* sensors are used to monitor the *RH* and *T* of the sample flow before and after the dryer unit. Silica gel desiccator is used to obtain a dry sheath air flow which in turn dries the main flow through the Nafion tube.

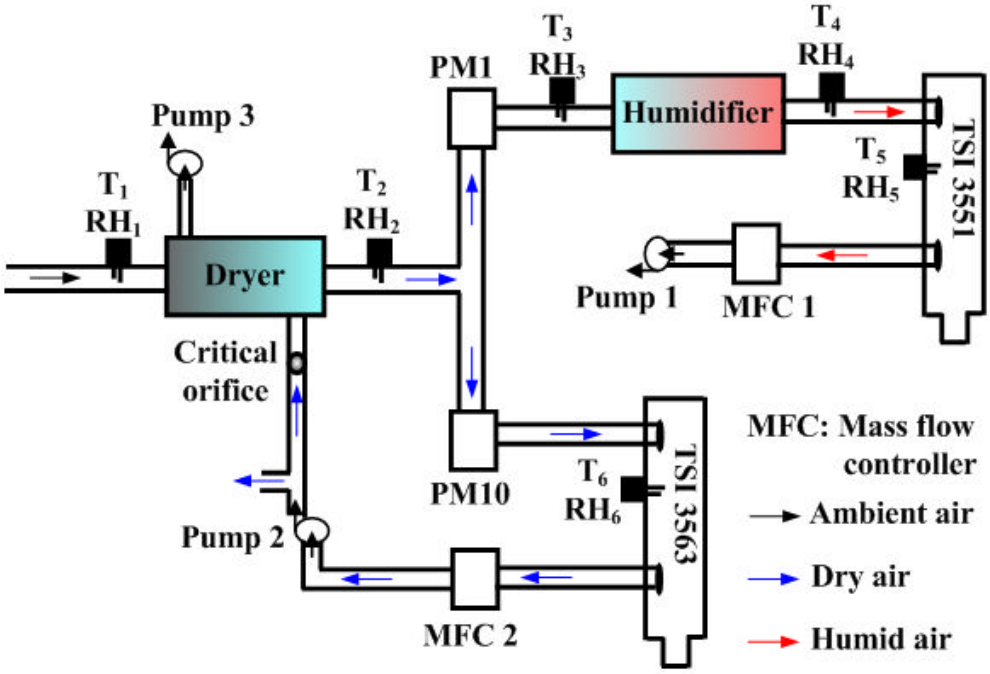

Figure A.4. The Humidograph system.

The dry flow is split into two channels both with a flow rate of 16.66 *LPM*. One channel is fed to a TSI three wavelength Integrating Nephelometer (IN-3563) with a PM 10 inlet. Another channel is fed to a Gore-Tex humidifier surrounded by a water jacket for varying the *RH* in a controlled way. The thick walls of the Gore-Tex tube have the property to permeate water vapour through them from the high vapour pressure side to the low vapour pressure side. *RH* and *T* sensors across the humidifier monitor the performance of the Humidifier unit and control the degree of humidification through a feed-back loop which regulates the temperature of the heating tape, wrapped around the water jacket, using a HORST temperature regulator.

The humid flow then enters a TSI single wavelength Integrating Nephelometer (IN-3551). Mass flow controllers (MFC) at the end of the Humidograph control the flow rate throughout the system.

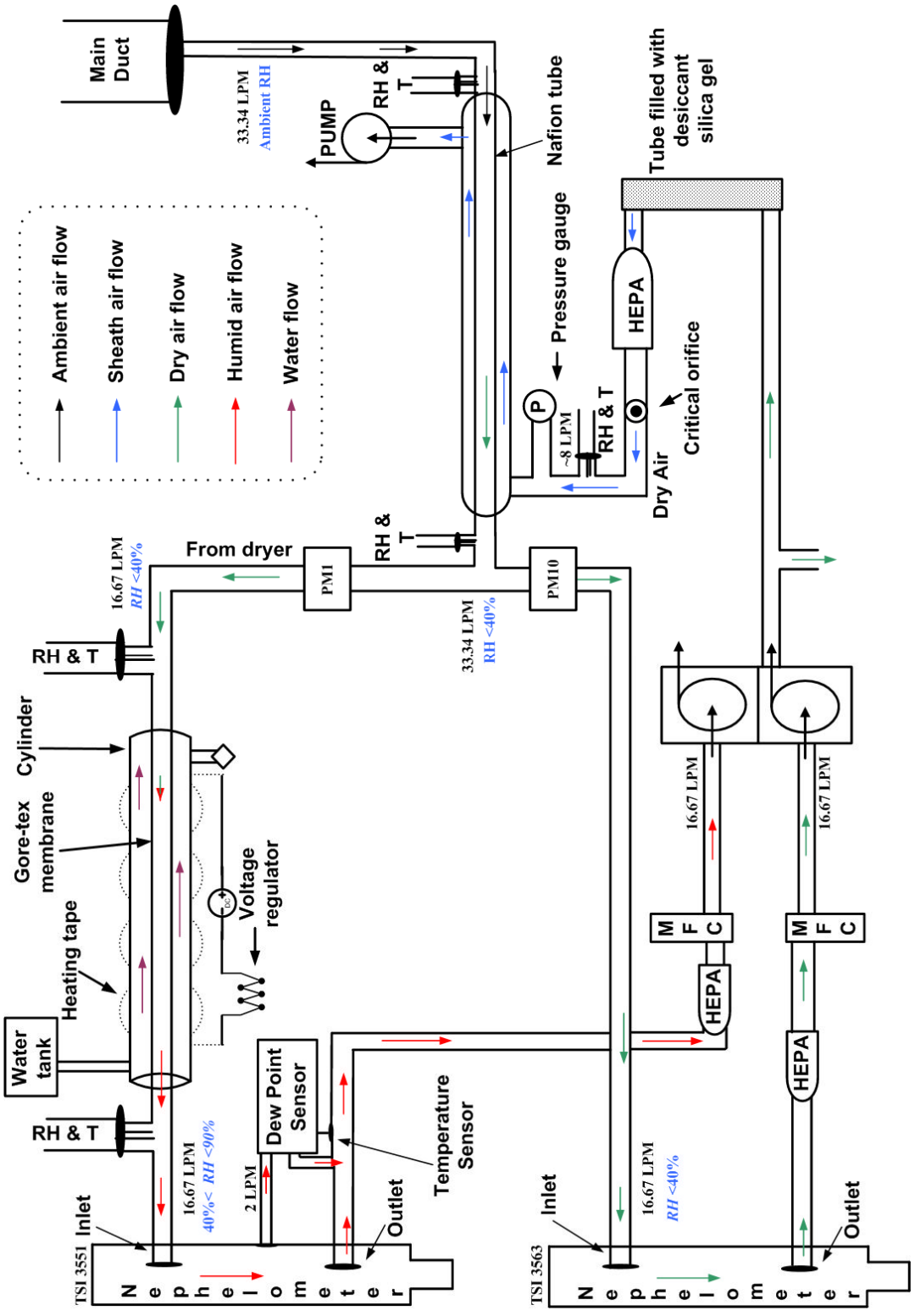

Figure A.5. Detailed diagram of the Humidograph system.

Figure A.6 outlines the modifications made (in red) to IN-3551 in order to reduce the temperature inside the Nephelometer measurement chamber. D denotes the dew-point chilled mirror sensor that is used to accurately measure the constantly changing *RH*.

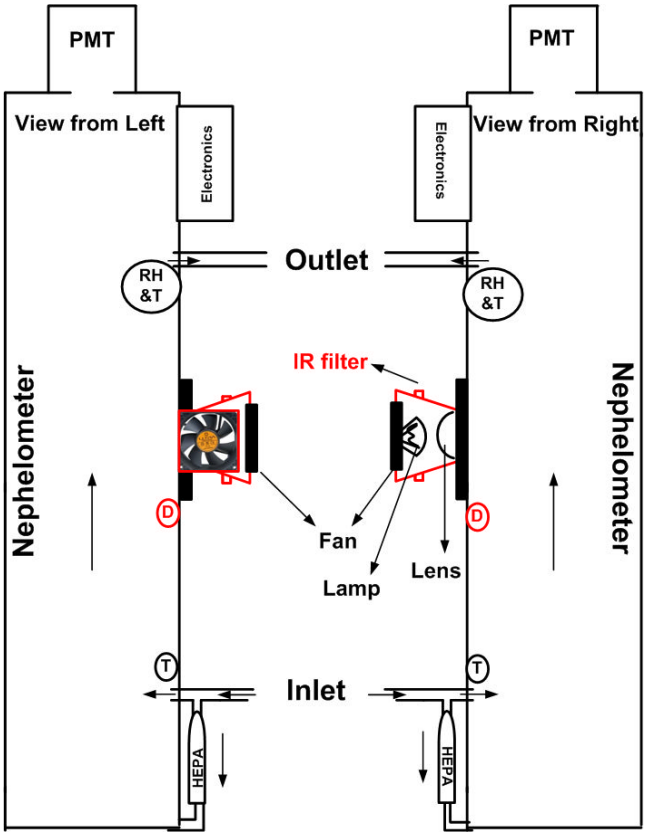

Figure A.6. Schematic of the modifications done to the Nephelometer.

A.3.1. IR filter test

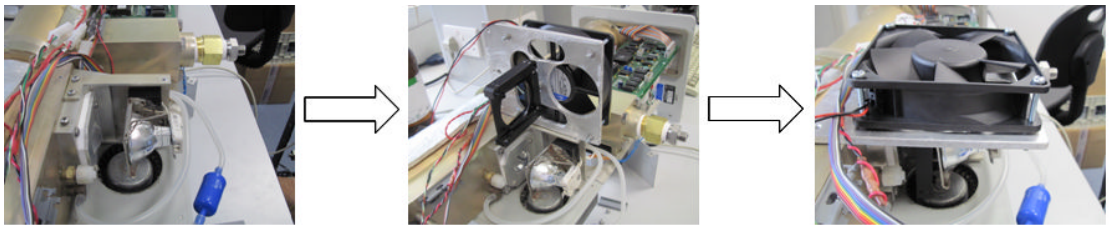

Figure A.7. Mounting the IR filter and cooling fan on the Nephelometer body.

Tests have been conducted to check the efficiency of the IR cut-off filter to effectively screen the heat radiation from reaching the Nephelometer measurement chamber. It was found that by placing the IR filter in between the

lamp and lens (Figure A.7), ΔT between the inlet and chamber was reduced by approximately 1.1^{0}C. Figure A.8 shows ΔT between the inlet and chamber of the Nephelometer with the IR filter in place and after removing it. ΔT can be further reduced by placing an additional fan to cool the IR cut-off filter (Figure A.7), as the filter gets hot due to continuous heat radiation from the lamp and hence may contribute to ΔT due to conduction of heat to the Nephelometer body.

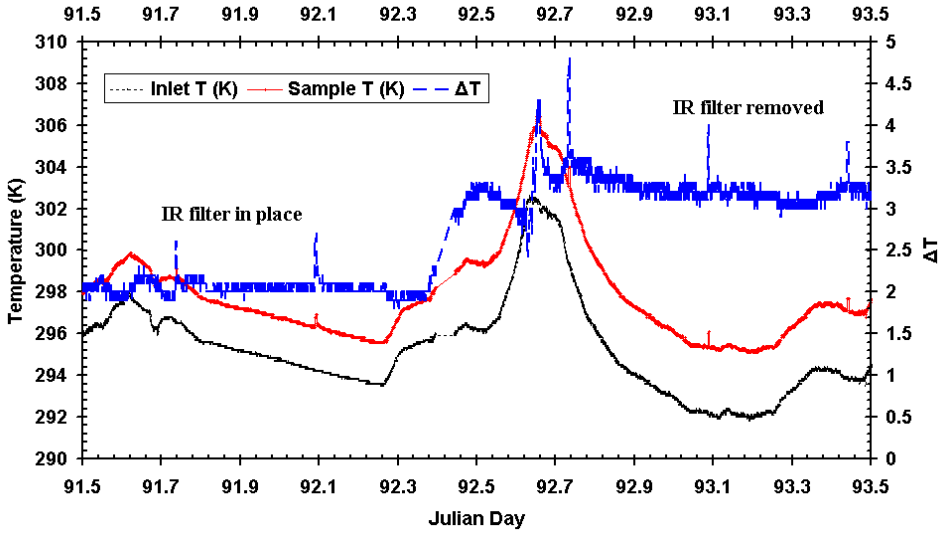

Figure A.8. Effect of an IR cut filter on the temperature difference between inlet and chamber.

A.3.2. Mass Flow Controller (MFC) test

A mass flow controller (MFC) is used in order to maintain a steady sample flow through the Humidograph system. We programmed the MFC to shut down automatically in the event of pump failure. This will prevent the MFC from overheating and thus will ensure that the control valves of the MFC are not damaged. As shown in Figure A.9, the dashed blue line shows the set point sample flow rate and the red solid line shows the corresponding actual flow through the MFC. The MFC flow rate closely follows the set point flow rate, with an accuracy of ± 0.05 *LPM*, and falls to zero the moment the set point flow rate is changed to zero (indicating failure of the pump).

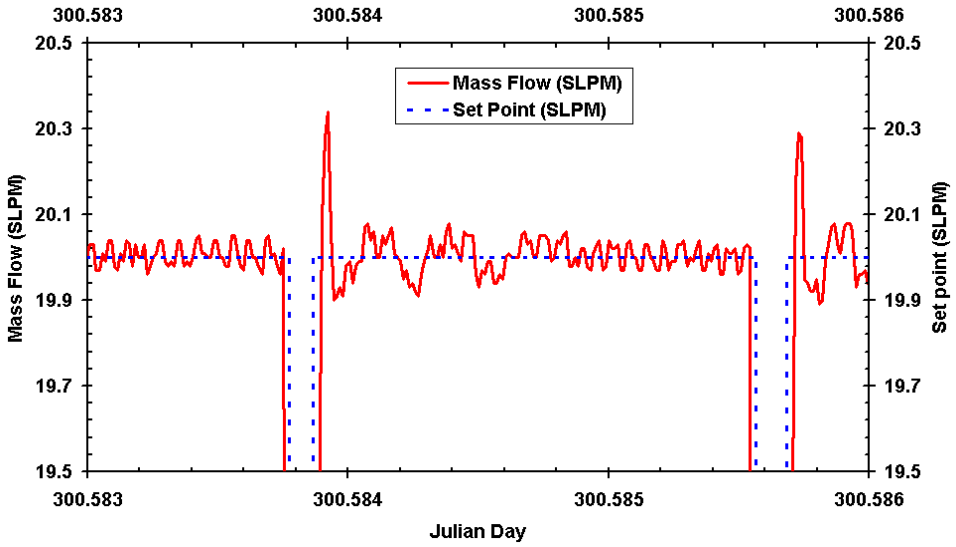

Figure A.9. Mass Flow Controller test.

A.3.3. Dryer test

A Nafion tube dryer is used to dry the sample flow to a defined low *RH* (< 45 %). The ratio between sheath flow to sample flow is kept at 1:4. Sheath flow is provided using a desiccant dryer which in turn is kept dry using a feed-back loop from the dry sample flow. Figure A.10 shows the variation of the ambient, sheath and after dryer *RH*. Though the ambient *RH* is 90-95 %, the Nafion dryer is able to effectively dry the sample flow to < 30 % *RH*.

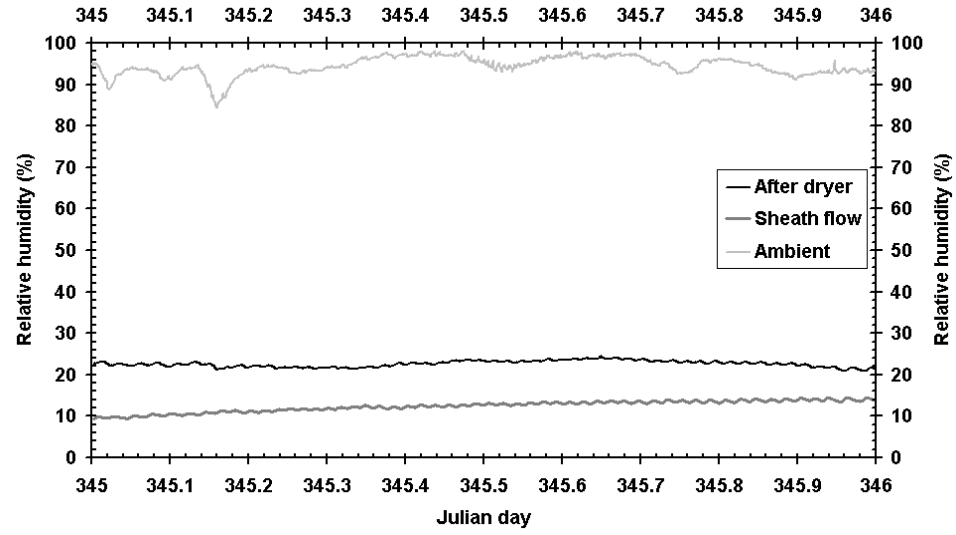

Figure A.10. Performance of the Dryer.

A.3.4. Humidifier test

A Gore-Tex tube humidifier has been built to humidify the sample flow to a desired *RH* level. For controlled humidification of the flow, a HORST temperature regulator is used. The heating tape heats up the water jacket surrounding the tube. Water vapour thus permeates through the wall of the Gore-Tex tube towards the lower vapour side, thus humidifying the sample flow. The temperature of the heating tape is thus directly related to the amount of humidification of the sample flow. Figure A.11 shows the percentage humidification as a function of temperature of the heating tape. Other factors which affect the rate of humidification are the sample flow rate and the ambient temperature. The sample flow rate is kept constant for this experiment at 16.6 *LPM*. The effect of ambient temperature was minimized by insulating the humidifier.

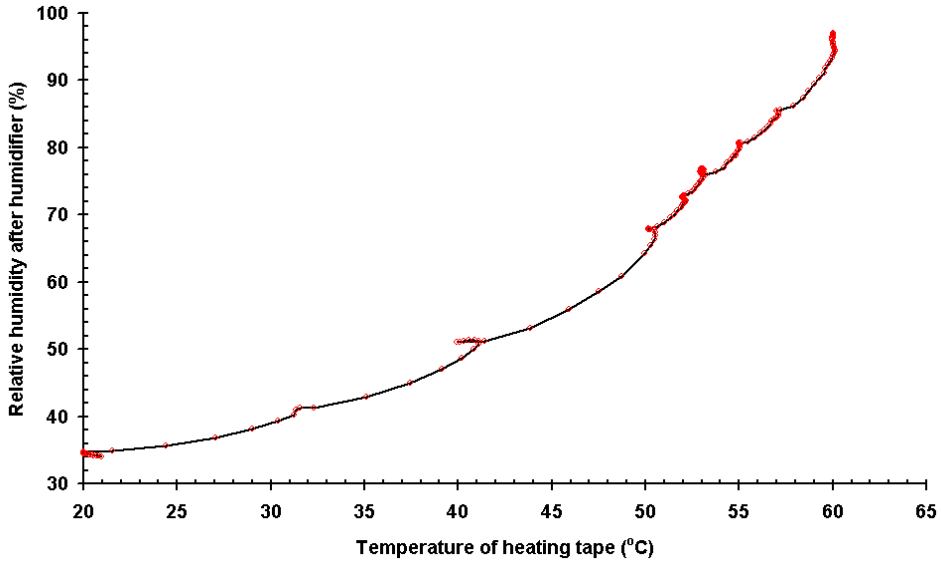

Figure A.11. Performance of the Humidifier.

A.3.5. Hygroclip performance test

A calibration setup was prepared for cross checking the performance of Hygroclip *T* and *RH* sensors using a Vaisala humidity meter calibrator HMK 11. Saturated salt solutions of *NaCl* and *LiCl* were prepared using standard procedures. A saturated solution of *NaCl* salt has a *RH* of 75.3% while that of *LiCl* salt has a *RH* of 11.3%, at 25.0 ^{0}C. Test results are shown in Figure A.12. Two Hygroclip *T* and *RH* sensors were tested for both salt solutions. Horizontal lines running parallel to the Julian day-axis show the standard *RH* values for the salt solutions at 25.0 ^{0}C. Both the sensors appear to deviate from the standard values by between 0.2% to 0.5% *RH* but are well within the standard accuracy of the sensors which is ± 0.8% *RH*.

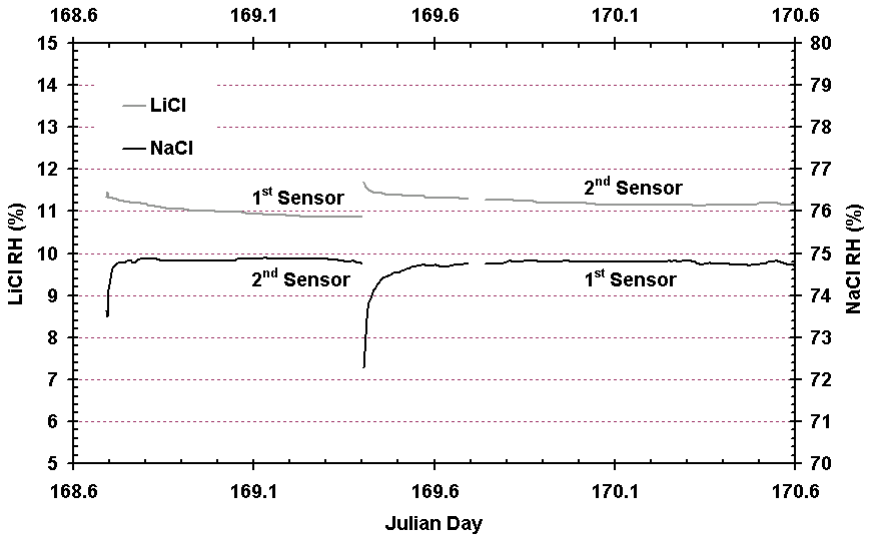

Figure A.12. Hygroclip performance test.

A.4. Software module for the Humidograph system

An efficient and well structured computer program (software) is required to enable synchronization between different instruments within the humidograph system. The program should also have the capability to operate and control the system as well as organize the data. One can classify the main functioning of the humidograph program in three broad categories, as shown in Figure A.13.

i. Setup of the humidograph: This includes defining the port address and parameters, Nephelometer measurement settings, flow rate, sampling and averaging time, location and initials of the file generated.

ii. Monitor & Control of the hardware: A major task for the program is to control *RH* and flow throughout the system, control the degree of humidification, and also to monitor the performance of different hardware units. Precipitation of water can damage the *RH* and *T* sensors and the measurement chamber of the Nephelometer. The program will cease the operation of humidification system in the event of *RH* overshoot.

iii. Real-time display: This section of program will display the real-time values of different parameters measured by humidity and temperature sensors, photo-multiplier tube, dew-point sensor, and also processed parameters from the Nephelometer.

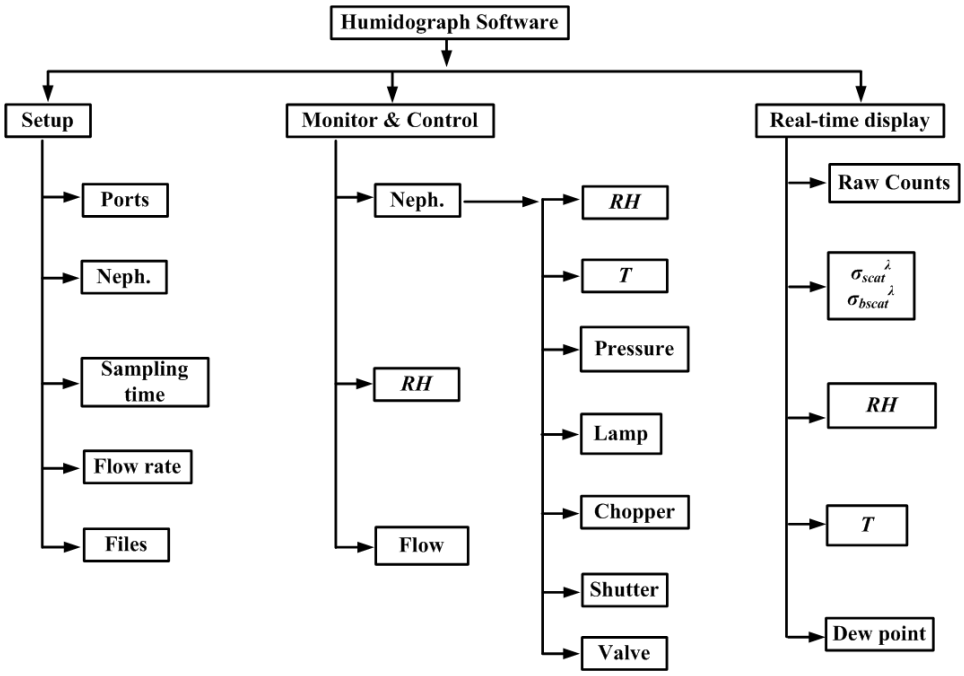

Figure A.13. Flow diagram showing major sections of the Humidograph software.

Software has been developed in LabVIEW, mainly to coordinate the functioning of different instruments used in the humidograph system. In addition to the above mentioned tasks, the software also takes care of the following:

i. Regulates the *RH* of the main flow through the humidifier.

ii. Shuts down the system in case of an *RH* overshoot which can damage the instruments.

iii. Prevents the Mass flow controllers, from excessive heating in the event of zero flow or pump failure, by switching them off.

iv. Data logging from different instruments into a single data file on a daily basis.

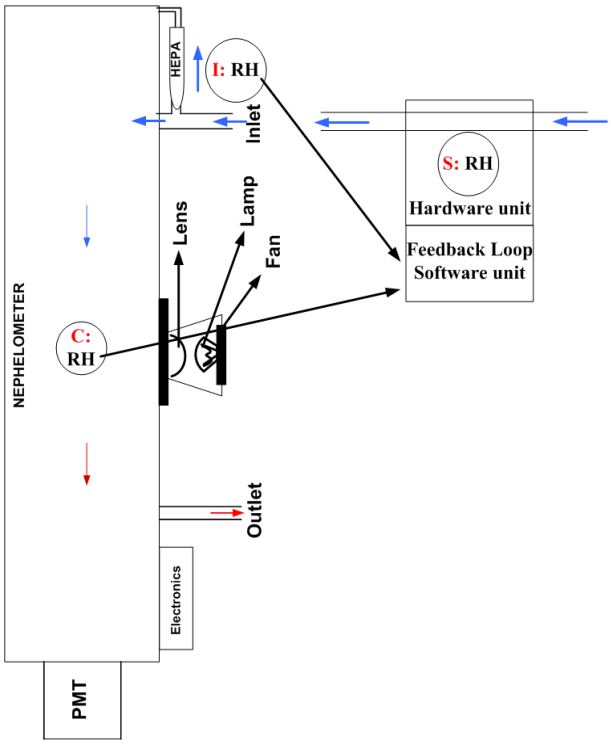

Figure A.14. Coordination between software and hardware units to control the *RH* of the sample flow.

One of the main tasks of the developed software is to effectively control the *RH* of the sample flow by sending appropriate commands to the hardware unit (HORST temperature regulator). Once we define the set-point *RH*, and measure the inlet and chamber *RH*, as shown in Figure A.14, the software unit will compute the step size (Figure A.15), using a proportional–integral–derivative (PID) function, to increase the temperature of the heating tape.

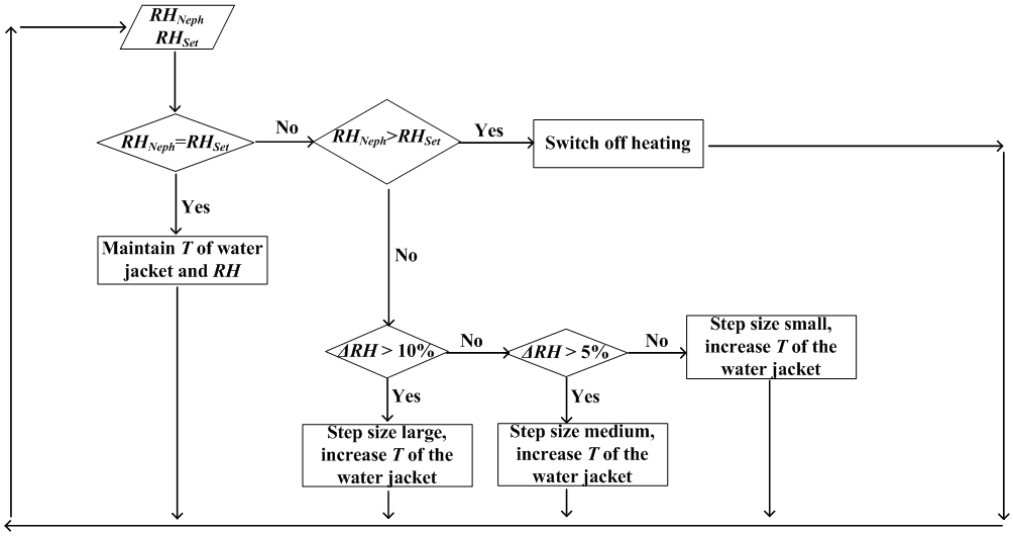

Figure A.15. Determining the step size to increase the temperature of the water jacket.

A tree-chart of the developed humidograph software is shown in Figure A.16. On the far left (1st column) is the 'WET NEPH' control which is the coordinator and the main program. The 2nd column consists of supporting programs which deal with a particular instrument or a specific feature of the instrument e.g. graph, Julian day etc. The rest of the columns contain graphical codes supporting certain features of individual instruments. Screenshots of the developed software are shown in Figures 5.17 – 5.19. The developed software makes it easier for a user to monitor the functioning of the instrument in near-real time on a remote desktop.

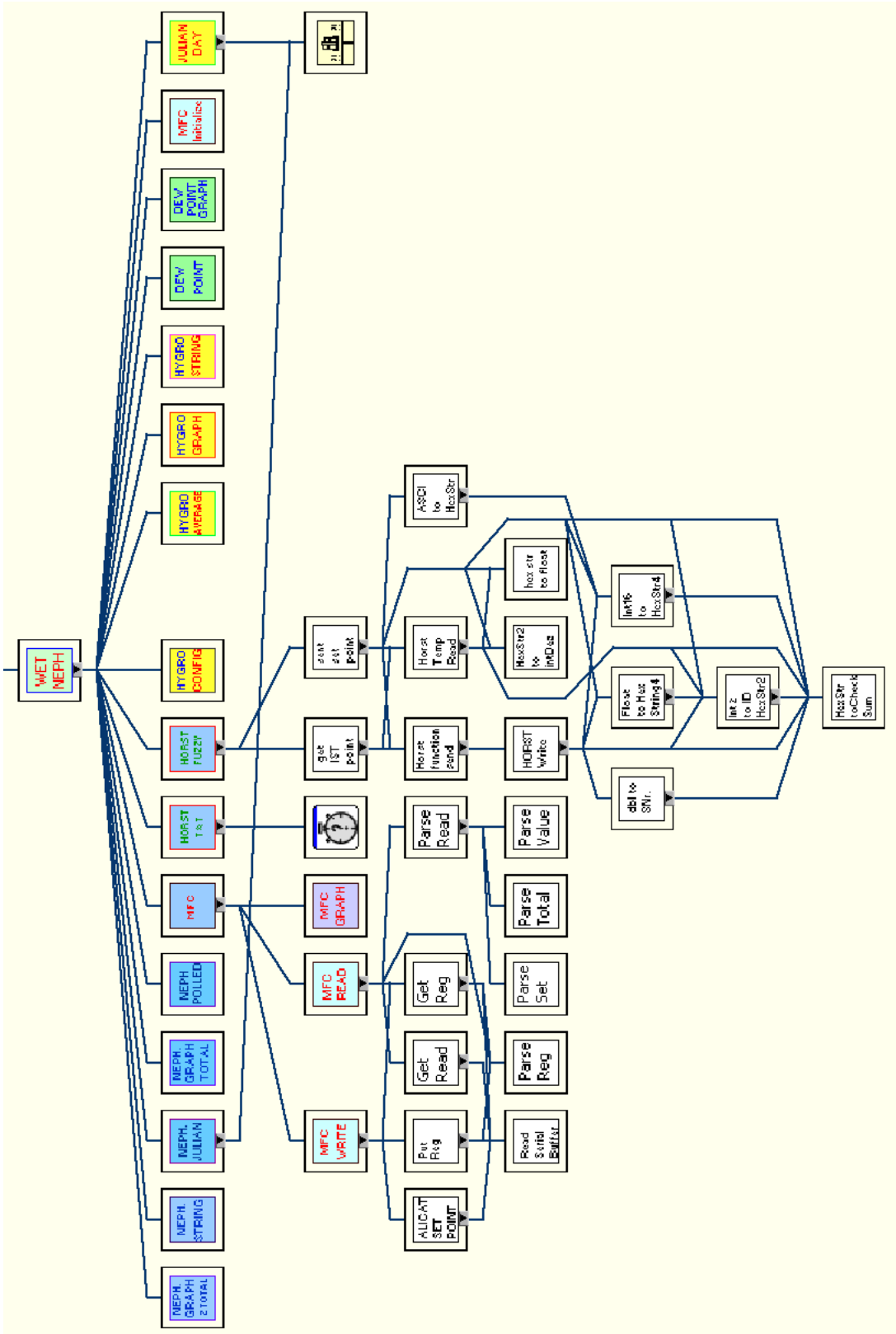

Figure A.16. Tree-chart of the developed Humidograph software.

A separate control tab is used to accommodate and display the Nephelometer parameters, as shown in Figure A.17. Apart from Nephelometer

status and data display, a separate graphical representation of the zero measurement is shown. This is for real time monitoring of the background noise level of the Nephelometer. Monitoring the background noise level is particularly important because it directly tells about the health of the instrument and indicates a requirement of servicing or calibration of the Nephelometer. The real time display of *RH*, *T* and dew point at different locations within the instrument is shown in Figure A.18.

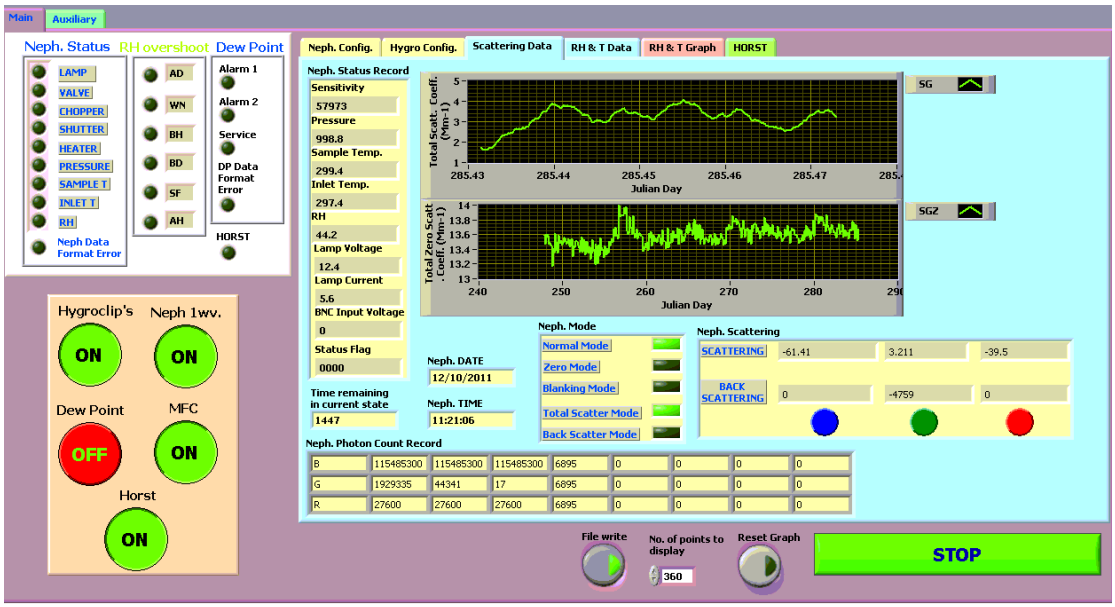

Figure A.17. Software module screenshot 1.

A separate section has been dedicated for the real time display of errors related to the instrument or data or other vital parameters as shown on the left hand side in Figure A.18. The first column in the Figure shows any error related to the functioning of the Nephelometer, while the second and third columns indicate the status of *RH*, as above or below threshold value, at different positions within the system. A control panel has been provided to operate and control individual instrument with the existing LabVIEW program without the need for running all the instruments together. This is particularly helpful during the testing phase when one needs to operate and monitor the performance of individual instruments. Also, this is helpful in the event if one or more instruments have to be switched off while the complete system is running.

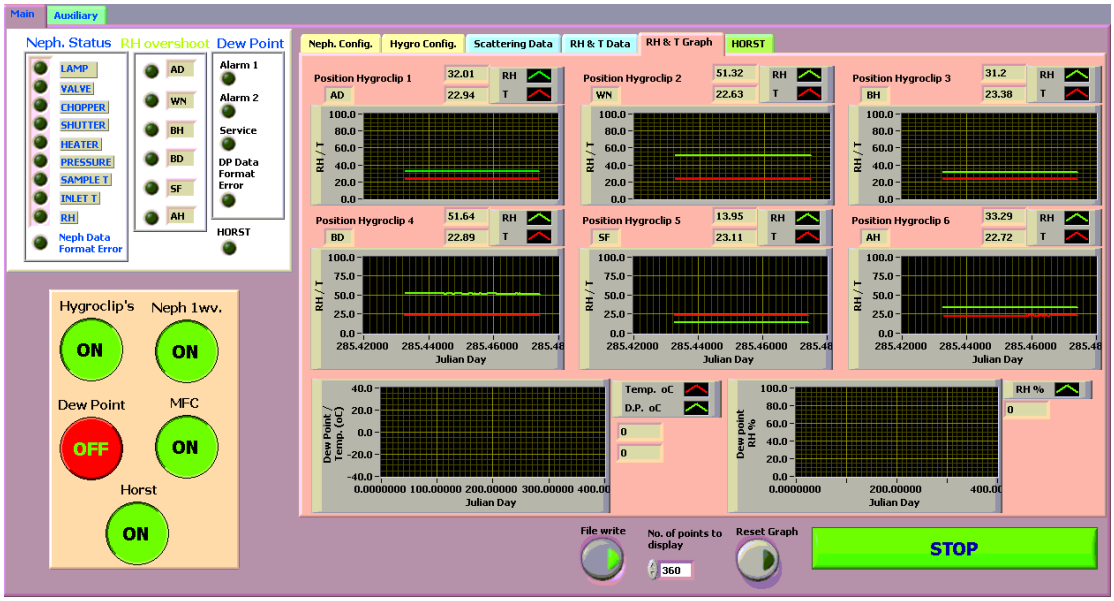

Figure A.18. Software module screenshot 2.

Auxiliary parameters are grouped into a separate tab as shown in Figure A.19. This consists of the file names and directory, MFC flows, port settings etc.

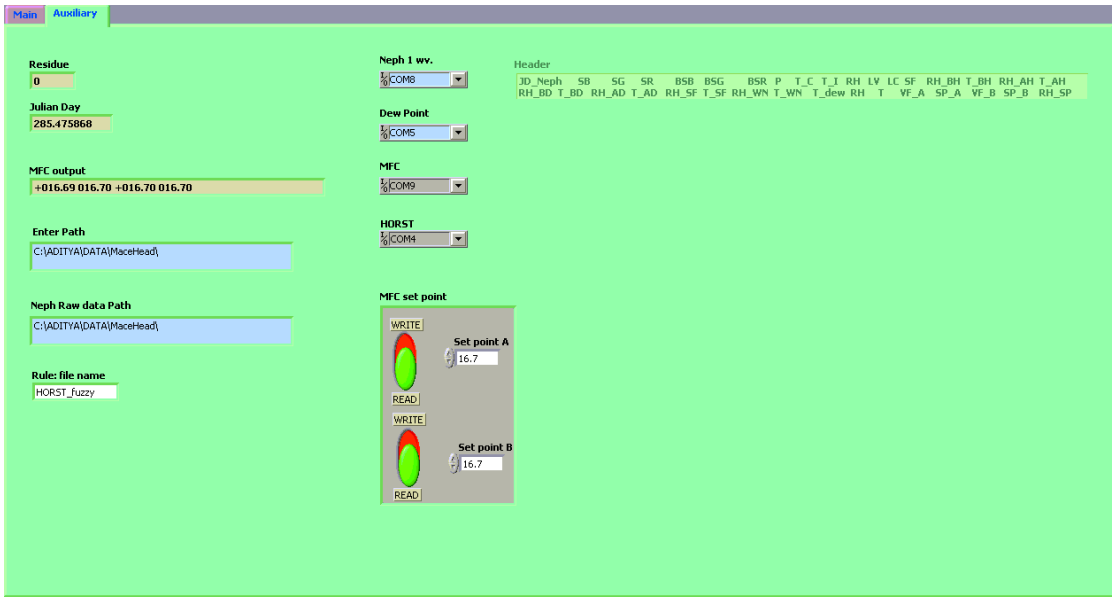

Figure A.19. Software module screenshot 3.

Figure A.20 shows the variation of *RH* at different locations within the Humidograph instrument. It also shows the performance of the dryer in effectively drying the sample flow and the performance of the humidifier and temperature controller units in maintaining and scanning the *RH* of the sample flow according to a set point *RH*.

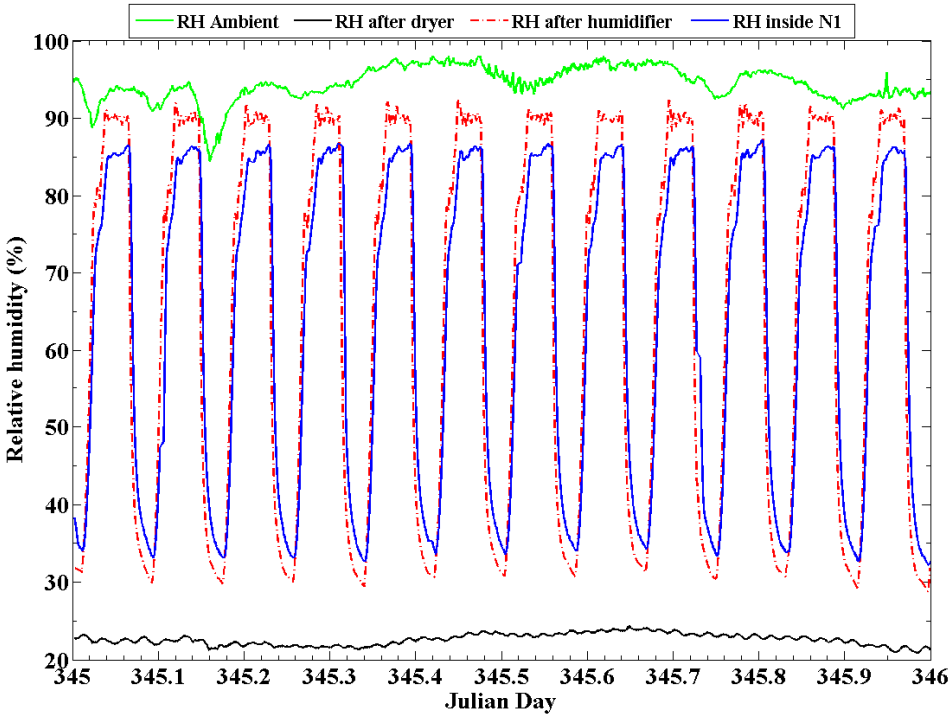

Figure A.20. Variation of *RH* at different stages inside the Humidograph system.

A.5. Laboratory results with standard salts

Tests have been conducted to ascertain the performance of the Humidograph system. Two salts (*NaCl* and $(NH_4)_2SO_4$) were tested for their deliquescence relative humidity (*DRH*). At deliquescence *RH* (*DRH*), the particle size and hence its scattering efficiency increases abruptly. A TSI model 3076 atomizer is used to atomize polydisperse aerosol particles. Size segregated aerosols were obtained by using a TSI model 3071 electrostatic classifier. The deliquescence *RH* of *NaCl* and $(NH_4)_2SO_4$ are 75.3 % and 79.5 % *RH*, respectively [*Tang and Munkelwitz*, 1993].

Initially the *DRH* of the *NaCl* was measured to be 61.6 % and that of $(NH_4)_2SO_4$ to be 71.8 %. These values are significantly below the *DRH* values mentioned above. This discrepancy was due to the following two reasons: i) the IR filter was not mounted on the Nephelometer during the experiment and hence the *RH* inside the Nephelometer measurement chamber dropped due to a warm atmosphere inside and ii) the most humid location where the deliquescence

occurs is downstream of the Humidifier. At this location the flow cools down and the *RH* of the flow is stable. Hence we colour coded the existing *f(RH)* values with the *RH* after the humidifier. The results are shown in Figure A.21 for *NaCl* and in Figure A.22 for $(NH_4)_2SO_4$, respectively. Actual deliquescence occurred at 75.8 % *RH* for *NaCl* and at 80.1 % *RH* for $(NH_4)_2SO_4$. These values closely follow the previously reported *DRH* values of 75.37 % for *NaCl* and 79.5 % for $(NH_4)_2SO_4$ by *Tang and Munkelwitz* [1993].

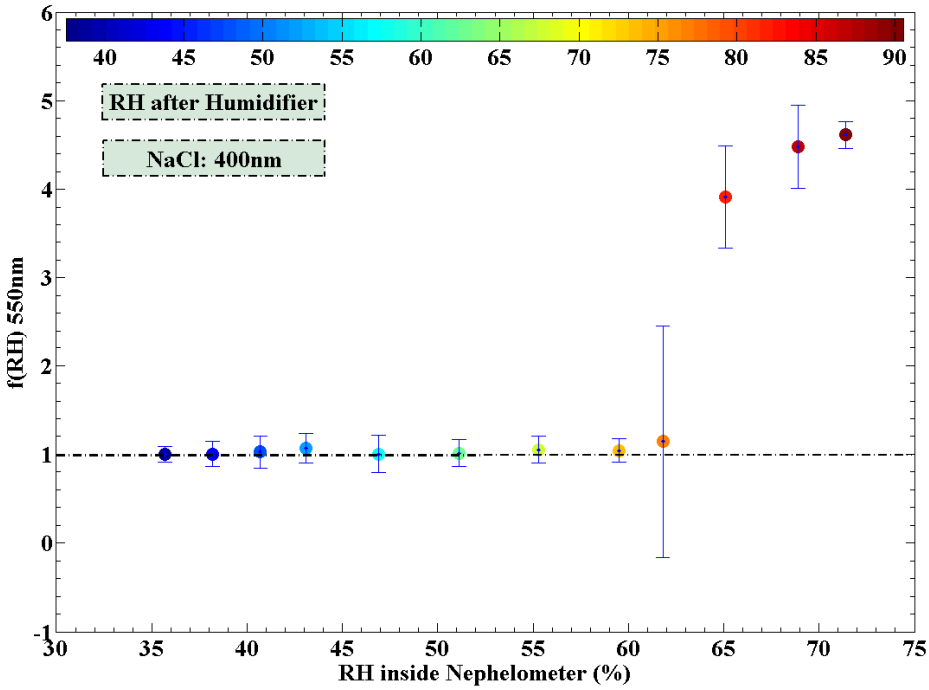

Figure A.21. Humidogram for 400nm *NaCl* test particles.

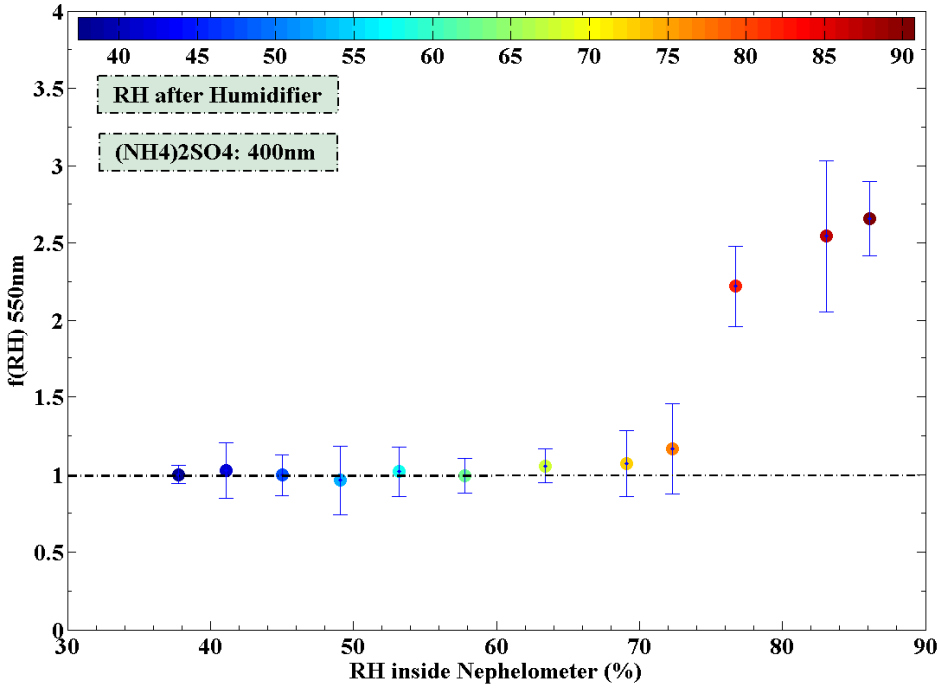

Figure A.22. Humidogram for 400nm $(NH_4)_2SO_4$ test particles.

References

Anderson, T. L., and J. A. Ogren (1998), Determining aerosol radiative properties using the TSI 3563 integrating nephelometer, *Aerosol Sci. Technol.*, *29*(1), 57-69.

Anderson, T. L., et al. (1996), Performance characteristics of a high-sensitivity, three-wavelength, total scatter/backscatter nephelometer, *J. Atmos. Oceanic Technol.*, *13*(5), 967-986, doi: doi:10.1175/1520-0426(1996)013<0967%3APCOAHS>2.0.CO%3B2.

Bodhaine, B. A., N. C. Ahlquist, and R. C. Schnell (1991), Three-wavelength nephelometer suitable for aircraft measurement of background aerosol scattering coefficient, *Atmos. Environ.*, *25 A*(10), 2267-2276.

Bond, T. C., D. S. Covert, and T. Muller (2009), Truncation and angular-scattering corrections for absorbing aerosol in the TSI 3563 nephelometer, *Aerosol Sci. Technol.*, *43*(9), 866-871.

Heintzenberg, J., and R. J. Charlson (1996), Design and applications of the integrating nephelometer: A review, *J. Atmos. Oceanic Technol.*, *13*(5),

987-1000, doi: doi:10.1175/1520-0426(1996)013<0987%3ADAAOTI>2.0.CO%3B2.

Heintzenberg, J., and G. Erfurt (2000), Modifacation of a commercial integrating nephelometer for outdoor measurements, *J. Atmos. Oceanic Technol.*, *17*(12), 1645-1650.

Kleefeld, C., C. D. O'Dowd, S. O'Reilly, S. G. Jennings, P. Aalto, E. Becker, G. Kunz, and G. De Leeuw (2002), Relative contribution of submicron and supermicron particles to aerosol light scattering in the marine boundary layer, *J. Geophys. Res.*, *107*(D19), doi: 10.1029/2000JD000262.

Müller, T., M. Laborde, G. Kassell, and A. Wiedensohler (2011), Design and performance of a three-wavelength LED-based total scatter and backscatter integrating nephelometer, *Atmospheric Measurement Techniques*, *4*(6), 1291-1303, doi: 10.5194/amt-4-1291-2011.

Müller, T., et al. (2009), Angular illumination and truncation of three different integrating nephelometers: Implications for empirical, size-based corrections, *Aerosol Sci. Technol.*, *43*(6), 581-586.

Quinn, P. K., T. L. Anderson, T. S. Bates, R. Dlugi, J. Heintzenberg, W. Von Hoyningen-Huene, M. Kulmala, P. B. Russell, and E. Swietlicki (1996), Closure in tropospheric aerosol-climate research: A review and future needs for addressing aerosol direct shortwave radiative forcing, *Contrib. Atmos. Phys.*, *69*(4), 547-577.

Quirantes, A., F. J. Olmo, H. Lyamani, and L. Alados-Arboledas (2008), Correction factors for a total scatter/backscatter nephelometer, *J. Quant. Spectrosc. Radiat. Transfer*, *109*(8), 1496-1503.

Ramaswamy, V., et al. (2001), Radiative forcing of climate change In: Climate Change 2001: The Scientific Basis. Contribution of Working Group I to the Third Assessment Report of the Intergovernmental Panel on Climate Change [Houghton, J.T.,Y. Ding, D.J. Griggs, M. Noguer, P.J. van der Linden, X. Dai, K. Maskell, and C.A. Johnson (eds.)], edited, Cambridge University Press, Cambridge, UK.

Rood, M. J., M. A. Shaw, T. V. Larson, and D. S. Covert (1989), Ubiquitous nature of ambient metastable aerosol, *Nature*, *337*(6207), 537-539.

Schwartz, S. E. (1996), The Whitehouse effect - Shortwave radiative forcing of climate by anthropogenic aerosols: An overview, *J. Aerosol Sci.*, *27*(3), 359-382.

Tang, I. N., and H. R. Munkelwitz (1993), Composition and temperature dependence of the deliquescence properties of hygroscopic aerosols, *Atmos. Environ.*, *27 A*(4), 467-473.